NASA CR-135162
R76AEG456

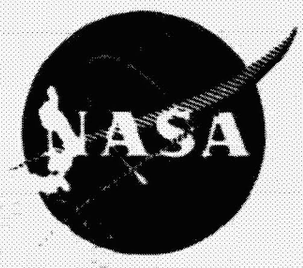

LINEARIZED BLADE ROW COMPRESSION COMPONENT MODEL

STABILITY AND FREQUENCY RESPONSE ANALYSES OF A J85-13 COMPRESSOR

BY

W.A. TESCH
R.H. MOSZEE
W.G. STEENKEN

GENERAL ELECTRIC COMPANY
AIRCRAFT ENGINE GROUP

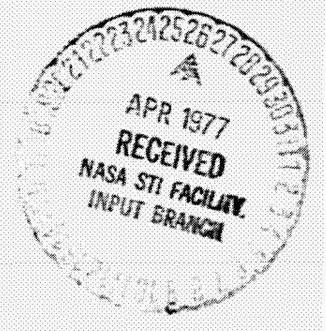

PREPARED FOR

NATIONAL AERONAUTICS AND SPACE ADMINISTRATION

NASA-LEWIS RESEARCH CENTER

CONTRACT NAS3-19854

1. Report No.	2. Government Accession No.	3. Recipient's Catalog No.
NASA CR-135302		

4. Title and Subtitle	5. Report Date
Linearized Blade Row Compression Component Model Stability and Frequency Response Analyses of a J85-13 Compressor	September 1976
	6. Performing Organization Code

7. Author(s)	8. Performing Organization Report No.
W.A. Tesch R.H. Moszee W.G. Steenken	R76AEG456
	10. Work Unit No.

9. Performing Organization Name and Address	11. Contract or Grant No.
General Electric Company Aircraft Engine Group Cincinnati, Ohio 45215	NAS3-19854
	13. Type of Report and Period Covered
12. Sponsoring Agency Name and Address	Contractor Report
National Aeronautics and Space Administration Washington, D.C. 20546	14. Sponsoring Agency Code

15. Supplementary Notes

Project Monitor: C.J. Daniele
NASA-Lewis Research Center, Cleveland, Ohio 44135

16. Abstract

NASA developed stability and frequency response analysis techniques have been applied to the General Electric Dynamic Blade Row Compression Component Stability Model in an effort to provide a more economic approach to surge line and frequency response determination than that provided by time-dependent methods. This blade row model was linearized and the Jacobian matrix was formed. The clean-inlet-flow stability characteristics of the compressors of two J85-13 engines were predicted by applying the alternate Routh-Hurwitz stability criterion to the Jacobian matrix. The predicted surge line agreed with the clean-inlet-flow surge line predicted by the time-dependent method to a high degree except for one engine at 94% corrected speed. No satisfactory explanation of this discrepancy has been found. The frequency response of the linearized system was determined by evaluating its Laplace transfer function. The results of the linearized-frequency-response analysis agree with the time-dependent results when the time-dependent inlet total-pressure and exit-flow function amplitude boundary conditions are less than 1 percent and 3 percent, respectively. The stability analysis technique was extended to a two-sector parallel compressor model with and without interstage crossflow and predictions were carried out for total-pressure distortion extents of 180°, 90°, 60°, and 30°. The 180°-extent results with no crossflow agree with the time-dependent results. As with all parallel compressors, the technique overpredicts the loss in surge pressure ratio for all extents of distortion. Inter-stage crossflow in stage 1 did not improve the accuracy of the loss in surge pressure ratio predictions. It was concluded from this study that where linearized stability and frequency response analysis are applicable, these analyses provide results with accuracies equivalent to the time-dependent model and offer economic advantages over the time-dependent model.

17. Key Words (Suggested by Author(s))	18. Distribution Statement
Compressor Stability Linearized Stability Analysis Blade Row Model Frequency Response	

19. Security Classif. (of this report)	20. Security Classif. (of this page)	21. No. of Pages	22. Price*
Unclassified	Unclassified	77	

*For sale by the National Technical Information Service, Springfield, Virginia 22151

FOREWORD

The program described in this report was conducted by the Aircraft Engine Group of the General Electric Company, Cincinnati, Ohio for the NASA Lewis Research Center, National Aeronautics and Space Administration under Contract NAS3-19854.

The program was carried out under the technical cognizance of Mr. C.J. Daniele of the NASA Lewis Research Center Dynamics and Controls Branch.

The contract effort was conducted at the Evendale Plant of the Aircraft Engine Group, Cincinnati, Ohio under the technical direction of Dr. W.G. Steenken with Mr. R.H. Moszee and Mr. W.A. Tesch being the prime technical contributors.

TABLE OF CONTENTS

LIST OF ILLUSTRATIONS

LIST OF ILLUSTRATIONS (Continued)

LIST OF ILLUSTRATIONS (Concluded)

LIST OF TABLES

NOMENCLATURE

A	-	Area
$\underline{A}$	-	Jacobian Matrix
$A_{i\beta}$	-	Area Nominal to Flow Direction
$\underline{B}$	-	Input Matrix
C	-	Absolute Velocity
$\underline{C}$	-	Output Variable Linear Relation Matrix
C_L	-	Lift Coefficient
C_Z	-	Axial Velocity
C_U	-	Absolute Tangential Velocity
F_B	-	Blade Force
F_D	-	Drag Force in Direction of Blade Entrance Flow
F_{DZ}	-	Axial Component of Drag Force
F_L	-	Blade Lift Force
F_T	-	Blade Tangential Force
FF	-	Flow Function
FV	-	Scale Factor
F.V.	-	Free Volume
$\underline{I}$	-	Identity Matrix
IGV	-	Inlet Guide Vane
L	-	Volume Length
L-A	-	Linearized Analysis
M	-	Mach Number
M	-	Number of Screen Mesh per Unit Dimension
N	-	Rotor Speed in Revolutions per Minute

NOMENCLATURE (Continued)

$N/\sqrt{\theta}$	-	Corrected Speed
P	-	Static Pressure
P_d	-	Dynamic Pressure (P_T - P)
P_M	-	Mean Static Pressure
P_T	-	Total Pressure
ΔPRS	-	Loss in Surge Pressure Ratio
R	-	Specific Gas Constant
$\underline{R}$	-	Output Variable Matrix
S_F	-	Entropy Production Term
T-D	-	Time Dependent
$\underline{T}$	-	Transformation Matrix
T_T	-	Total Temperature
U	-	Pitch Line Wheel Speed
V	-	Volume
W	-	Flow Rate
$\underline{W}$	-	Numerator Matrix of Transfer Function
W_c	-	Corrected Flow
W'	-	Relative Velocity
X	-	Generalized State Variable
Y	-	State Variable at Equilibrium Operating Point
$\underline{Z}$	-	Transform State Variable Vector
a_T	-	Stagnation Velocity of Sound
f	-	Frequency
f(X)	-	Function of (X)

NOMENCLATURE Continued)

g_o	-	Gravitational Constant
i	-	Incidence Angle
j	-	$\sqrt{-1}$
l	-	Kinetic Pressure, $1/2\ \rho\ (W')^2$
r	-	Pitch-line Radius
r	-	Transformed Output Variable
s	-	Specific Entropy
s	-	Laplace Transform Dummy Variable
t	-	Time
$\underline{u}$	-	Forcing Function Vector
α,β	-	Blade Inlet or Exit Air Angles (Absolute and Relative, Respectively)
α^*,β^*	-	Blade Inlet or Exit Metal Angles (Stator and Rotor, Respectively)
β_c	-	Lift Direction Vector Correction Angle
β_∞	-	Lift Direction Vector Angle
γ	-	Ratio of Specific Heats for Air
δ	-	Deviation Angle
ϵ	-	Small Quantity
η	-	Efficiency (ψ_m/ψ_m')
θ	-	T_T/T_{STD}
ξ	-	Dummy Variable
ρ	-	Density
Φ	-	Flow Coefficient $\left(\frac{C_{z_i}}{2\pi N r_i}\right)$
ψ_m	-	Work Coefficient $\frac{\frac{\gamma}{\gamma-1}\, g_o R\ (T_{T_{i+1}} - T_{T_i})}{[2\pi N(r_i)]^2/2}$

NOMENCLATURE (Concluded)

ψ'_m	-	Pressure Coefficient $\dfrac{\frac{\gamma}{\gamma-1} g_o R T_{T_i}\left[\left(\frac{P_{T_{i+1}}}{P_{T_i}}\right)^{(\gamma-1)/\gamma} - 1\right]}{[2\pi N(r_i)]^2/2}$
$\bar{\omega}'$	-	Relative Total-Pressure Loss Coefficient
$\mathcal{L}$	-	Laplace Transform Operator
Underline	-	Vector Quantity
$\cdot$	-	Scalar Product
x	-	Vector Product

SUBSCRIPTS

2	-	Compressor Entrance Station
3	-	Compressor Discharge Station
4	-	Turbine Diaphragm Station
T	-	Total
e	-	Equilibrium Operating Point
i	-	i-th Station
k	-	k-th Volume
m	-	m-th Stage
n	-	Number of Input Forcing Functions

SUPERSCRIPTS

$\overline{\quad\quad}$	-	Volume Average
'	-	Relative Frame of Reference
$\cdot$	-	Derivative with Respect to Time
T	-	Transpose of Matrix

1.0 SUMMARY

The objectives of this program were to adapt the General Electric Dynamic Blade Row Compression Component Stability Model for use with NASA developed linearized stability analysis and frequency response analysis subroutines and to demonstrate that these analysis techniques, which are used primarily in control analyses, give results which are equivalent to the time-dependent solution of the nonlinear equations describing the flow in a compression component.

Verification of the applicability of these techniques was carried out by comparing results with previously obtained NASA J85-13 engine data and with previously conducted time-dependent studies using the above mentioned General Electric model. The equations of this model were linearized about an equilibrium operating point resulting in a matrix, A, known as the Jacobian matrix. Based on the first method of Liapunov, the stability of the system was determined by either examining the signs of the real parts of the roots of the A matrix characteristic equation using the alternate formulation Routh-Hurwitz stability criterion or by actually solving for the eigenvalues and examining the signs of the real parts of the roots. The frequency response analyses were conducted using the A matrix and an input matrix B in conjunction with the NASA supplied subroutines which determined the linearized system transfer function using Laplace transforms.

The J85-13 clean-inlet-flow surge line was determined for each of two engines: one at 80, 87, 94, and 100 percent corrected speeds and the other at 87, 94, and 100 percent corrected speeds. The resulting 87 x 87 A matrices were tested for stability and the predicted surge line accurately matched the experimental data and the time-dependent model results except for the first engine at 94 percent speed. The cause of this anomaly is not understood. The stability characteristics of the other engine were accurately predicted.

The linearized frequency response analyses were conducted on the first engine with inlet-total-pressure oscillations and with exit-flow-function oscillations over the 0.1 to 200 Hz frequency range for 25 frequencies. These results were compared with time-dependent-solution results at frequencies of 30, 60, 100, 150, and 200 Hz. It was found that essentially identical results were achieved when the time-dependent model total-pressure oscillations were equal to ±0.5 percent of the mean inlet total pressure or when the exit-flow-function oscillations were equal to ±1.0 percent of the mean exit flow function.

Stability predictions were made for one-per-rev inlet total-pressure distortions at 80, 87, and 100 percent corrected speeds. A two-sector parallel compressor model was used and resulted in a 187 x 187 A matrix. At each speed, surge point predictions were made for total-pressure distortions produced by a 42 percent blockage screen with angular extents of 180°,

90°, 60°, and 30° and by a 49 percent blockage screen with angular extents of 180°, 90°, and 60°. The 180° angular extent stability analysis results were compared to existing time-dependent model solutions and this comparison showed that equivalent results were obtained. The stability analyses, in general, produced results which were in keeping with other parallel compressor results. That is, the loss in surge pressure ratio is overpredicted especially at low speeds (80 and 87 percent) where the speed lines have lower slopes. In an effort to improve the distorted-flow stability predictions, inter-stage axial-gap crossflow from the high total-pressure sector to the low total-pressure sector was simulated at one axial location in the compressor. The amount of crossflow was determined by obtaining the best match of the predicted distortion attenuation characteristics with the measured distortion attenuation characteristics for a 180° total-pressure distortion at corrected speeds of 80- and 100-percent. Crossflows for other extent distortions were scaled from these results based upon area ratios. It was found that crossflows at rotor 1 exit of 1.2 percent and 1.0 percent of sector inlet physical flow at 80 and 100 percent corrected speeds, respectively, gave the best match to the measured attenuation characteristics. Even though this mismatching of stages would significantly move the operating point of the low total-pressure sector in many cases, the mean compressor behavior at surge (loss in surge pressure ratio) was not improved and in some cases was worsened due to unrealistic sector speed line shapes. Use of a stage prediction method in such cases is necessary since the distorted sector may never reach the clean-inlet-flow surge line due to the stage mismatching. The linearized stability and the frequency response analyses employed in this study gave results which were equivalent to time-dependent solutions of the nonlinear set of equations. Such analyses offer significant economic advantage when linearized analyses are applicable.

2.0 INTRODUCTION

One of the most significant parameters of concern in the design and operation of gas turbine engines is surge margin. Aircraft engine designers are continually striving to provide adequate surge margin to insure successful steady- and transient-engine operation. Experience has revealed that surge margin can be degraded by a variety of factors such as deterioration, control tolerances, Reynolds number, stator misrigging, accelerations, inlet distortion, etc. Of these factors, one of the largest and most variable consumers of surge margin is inlet distortion.

Since it is not feasible to experimentally determine the response of a compression component or an engine to all possible combinations of distortion, the need has evolved whereby the stability (surge) of a compression component can be analytically predicted. There have been a number of recent studies using time-dependent methods. References 1 and 2 report the results obtained using stage by stage models and Reference 3 reports the results obtained by using a blade-row by blade-row model. As the models have become more complex, it has been necessary to turn from analog or hybrid computation to strictly digital computation. Even for very efficient solutions of the time-dependent equations such as that used in the Reference 3 study, computation costs represent a significant proportion of the effort. An approach (References 4 and 5) has been developed at NASA Lewis Research Center which potentially offers significant cost reductions.

This approach involves linearizing the nonlinear coupled system of equations which describe the compression system about an equilibrium operating point. This operation results in a matrix, the characteristic equation of which can be examined for the sign behavior of the real part of its roots. Instability will occur when any root has a positive real part. Further, it has been shown that these instabilities occur only at the experimentally determined surge line. Based on the first method of Liapunov, the nonlinear system of equations will be stable if the linear system of equations is stable. As explained in Reference 4, the stage by stage analytical representation of a compressor as given in Reference 1 was used and the resulting system of equations were then linearized. The stability of the resulting linear system which represented a J85-13 compressor was determined. The results showed good agreement between the analytically and experimentally determined surge lines.

The objectives of the program were to adapt the NASA developed technique for predicting surge in a compression component for use with the exisiting General Electric Dynamic Digital Blade Row Compression Component Stability Model (Reference 3) and to perform an evaluation of the capabilities of this stability analysis technique by comparing these results to time-dependent solution results and test data reported upon in Reference 3. These objectives were to be met by determining the clean-inlet-flow surge points for a J85-13 turbojet engine known as the "Moss" engine at the 80, 87, 94, and 100 percent corrected speed lines. Then the response of the

J85-13 compression component to inlet-total-pressure and exit flow-function oscillations over the 0.1 to 200 Hz frequency range was to be determined. The amplitude and phase angle results were to be compared with the results of the Reference 3 time-dependent program at five frequencies in the 20 to 200 Hz frequency range. The method was then to be extended to predicting the point of instability with distorted inflow conditions by using a system of equations describing a two sector parallel compressor. Stability predictions for a moderate level of distortion with angular extents of 30, 60, 90, and 180 degrees and for a higher level of distortion with angular extents of 60, 90, and 180 degrees were to be conducted at 80, 87 and 100 percent corrected speeds. Each of these cases was to be run with and without circumferential crossflow.

In this report, the methods used in the course of the study are reviewed and the results obtained in the course of the stability and frequency response predictions are discussed.

3.0 ANALYTICAL METHODS AND J85-13 ENGINE COMPRESSOR MODEL

The analytical formulation of the Dynamic Digital Blade Row Compression Component Stability Model and the methods employed in this study to determine the stability of the system of equations are reviewed. Further the J85-13 engine which is being simulated, the source of the blade row characteristics, and the manner in which the compression system is broken into volumes are discussed.

3.1 DESCRIPTION OF BLADE ROW MODEL

This review of the Dynamic Digital Blade Row Compression Component Stability model is taken from References 3 and 6. The complete set of nonlinear partial differential equations which describe the transfer and storage of mass, momentum, and energy within a fluid are called the equations of change. These equations have been integrated once over an arbitrary volume of the flow system to obtain the macroscopic balances for quasi one-dimensional flow without heat transfer and are reproduced below in the form in which they are used in the dynamic compression component model.

$$\frac{\partial \bar{\rho}_k}{\partial t} = \frac{1}{V_k} (W_i - W_{i+1}) \tag{1}$$

$$\frac{\partial \bar{W}_k}{\partial t} = \frac{g_o}{L_k} \left[\frac{W_i C_{z_i}}{g_o} - \frac{W_{i+1} C_{z_{i+1}}}{g_o} + P_i A_i - P_{i+1} A_{i+1} - P_M (A_i - A_{i+1}) + F_B \right] \tag{2}$$

$$\frac{\partial \overline{\rho s}_k}{\partial t} = \frac{1}{V_k} [W_i s_i - W_{i+1} s_{i+1} + S_F] \tag{3}$$

The subscripted variables on the right-hand side of the equations refer to quantities at the inlet (i) and exit (i+1) of the control volume. Variables on the left-hand side refer to volume averaged quantities, i.e., in generalized form

$$\bar{\xi} = \frac{\int \xi \, dV}{\int dV} \tag{4}$$

The energy equation (Equation 3) was derived by combining the equation of change for energy and one of the thermodynamic T ds relationships.

This set of equations (other than being applicable to quasi one-dimensional flows without heat transfer and to a finite, but small volume) properly and exactly describes the state of a fluid in motion. In order to solve Equations 1 through 3, it is necessary to supply the caloric and thermal equations of state and expressions for F_B (Blade Force), P_M (Mean Pressure), and S_F (Entropy Production).

In the following paragraphs, the blade force, mean pressure, and entropy production terms are discussed.

The blade force F_B of Equation 2 represents the blade force acting upon the fluid. The blade force can be determined through reference to the following sketch:

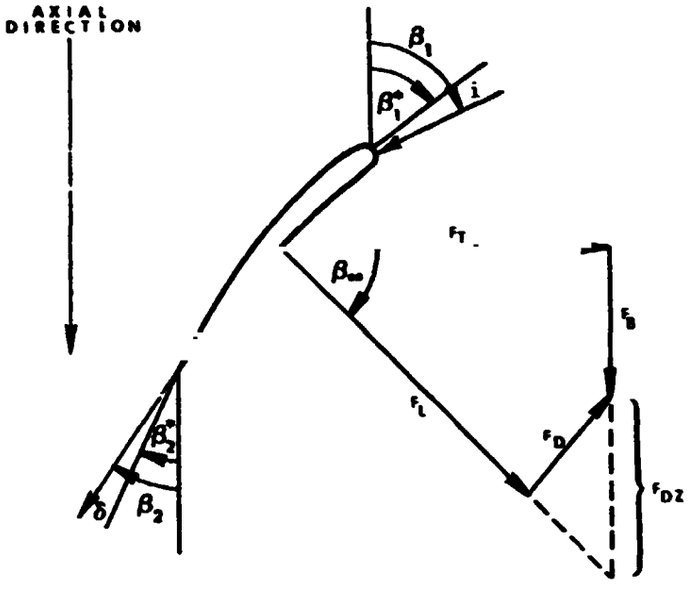

$$F_B = F_T \tan \beta_\infty - F_{DZ} \tag{5}$$

where

$$F_T = \frac{2}{g_o} \left(\frac{r_{i+1} W_{i+1} C_{U_{i+1}} - r_i W_i C_{U_i}}{r_i + r_{i+1}} \right) \tag{6}$$

and is derived from the Euler Turbine Equation. The direction of the lift vector is assumed to be

$$\beta_\infty = \frac{1}{2} \left(\beta_i + \beta_{i+1} \right) \tag{7}$$

The drag force (F_D) is obtained from the following equation

$$F_D = \bar{\omega}' \frac{P_i'}{P_{T_i}'} \frac{P_{d_i}'}{q_i'} (A_{i\beta} \cdot q_i') \tag{8}$$

which is based upon an analogy with the drag coefficient for duct flows. It is noted that the drag force acts in the direction of the inlet flow β_i. The term F_{DZ} in Equation 5 is then obtained from the relation

$$F_{DZ} = F_D \frac{[\cos(\beta_i - \beta_\infty)]}{\cos \beta_\infty} \tag{9}$$

where the numerator transforms the force (F_D) in the flow direction to a force along the mean chord line perpendicular to the lift vector and the denominator transforms that resultant force to an axial force.

It should be noted that in steady flow a momentum balance, in general, will not give the same total-pressure rise per stage as does an energy balance. The latter is assumed to be correct. The reason for this difference is that the proper direction of the blade lift vector is not exactly the arithmetic average of the flow angles (Equation 7). Comparison of the steady-state momentum and energy balance solutions permits the determination of a small "correction angle" which can then be added to β_∞ to give the proper lift direction. Hence, in actuality the lift direction angle is written as

$$\beta_\infty = 1/2 (\beta_i + \beta_{i+1}) + \beta_c \tag{10}$$

Equation 7, then, is replaced by Equation 10.

The mean pressure P_M of Equation 2 represents the average of the integral of the pressure distribution over the lateral surface area of the volume element as sketched below:

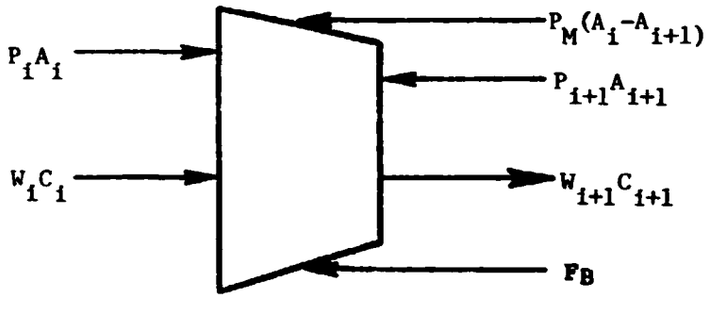

Although an analytical expression for the mean pressure acting on lossless, blade free volumes in steady flow can be derived, it leads to redundancy in the system of equations describing unsteady flow. Therefore, based upon steady-state momentum-balance analyses, an approximate linear expression for calculating blade-free volume mean pressure as a function of area convergence and inlet and exit pressures has been established for the J85-13 compressor model. Its form in terms of a scale factor (FV) for zero-swirl free volumes is given by the following equation:

$$P_M = P_i + FV\ (P_{i+1})\ /\ (1 + FV) \tag{11}$$

Similarly, an additional correlation was established for the non-zero swirl free volume between the IGV and the first rotor as a function of IGV exit air angle. It should be noted that the correlations are given in Reference 3 and are unique to this formulation and the J85-13 compressor. They are probably valid only for other compressors with similar Mach numbers and area changes.

For blade-row volumes, investigations have revealed that a good approximation for the mean pressure is two-thirds the higher of the inlet or exit static pressures plus one third the lower pressure. Deviations from this approximation are accounted for in the lift direction correction angle.

The term S_F in Equation 3 represents the total rate of irreversible conversion of mechanical to internal engergy and, in the case of this model, represents the entropy production due to blade row losses. It can be obtained from the expression:

$$S_F = \bar{W}R \ln \frac{\left(P'_{T_{i+1}} / P'_{T_i} \right)_{ideal}}{\left(P'_{T_{i+1}} / P'_{T_i} \right)_{actual}} \tag{12}$$

where the ideal relative total-pressure ratio which accounts for the change in pitch line radius from the entrance of a rotor blade row to its exit is written as

$$\left(\frac{P'_{T_{i+1}}}{P'_{T_i}} \right)_{ideal} = \left\{ 1 + \frac{\gamma - 1}{2} M_T^2 \left[1 - \left(\frac{r_i}{r_{i+1}} \right)^2 \right] \right\}^{\gamma/(\gamma - 1)} \tag{13}$$

M_T is equal to the ratio of the blade-row-exit pitch-line wheel speed to the inlet relative stagnation velocity of sound ($2\pi Nr_{i+1}/a_{T_i}$). In the case of a stator, the ideal relative total-pressure ratio is equal to one. The actual relative total-pressure ratio requires knowledge of the relative total-pressure loss coefficient which is defined as

$$\bar{\omega}' = \frac{P\hat{T}_{i+1}\Big)_{ideal} - P\hat{T}_{i+1}\Big)_{actual}}{P\hat{T}_i - P_i} \tag{14}$$

Equation 14 can be rewritten in the form

$$\frac{P\hat{T}_{i+1}}{P\hat{T}_i}\Bigg)_{actual} = \frac{P\hat{T}_{i+1}}{P\hat{T}_i}\Bigg)_{ideal} - \bar{\omega}' \left\{ 1 - \left[\frac{1}{1 + \frac{\gamma - 1}{2} (M_i')^2} \right] \right\}^{\gamma/(\gamma - 1)} \tag{15}$$

Hence, Equations 13 and 15 when substituted into Equation 12 provide complete definition of the entropy production term.

As might be expected, the input to the program, in addition to physical speed, inlet conditions and compressor geometry, requires the relative total-pressure loss coefficient ($\bar{\omega}'$) for each blade row, the deviation angle (δ) for the rotors, the correction angle (β_C) for both the rotors and stators. The relative total-pressure loss coefficient and the deviation angle are derived from stage-stacking results and are based upon clean-inlet-flow test data obtained by throttling at constant speed. The correction angle is obtained by comparing steady-flow force and energy balance solutions on a blade-row basis. These parameters can be represented as functions of incidence angle and are input to the program in this manner. These parameters, in conjunction with the velocity triangles and other ancillary relations, permit the determination of the thermodynamics of the fluid at each station. Blade-free volumes are treated as lossless volumes with no imposed blade force; hence, the F_B and S_F terms of Equations 2 and 3 are identically zero.

Time dependent solution of the system of equations (Equations 1 through 3 and the relations for F_B, P_M, and S_F) that comprise the dynamic digital compression component model is effected through a Taylor series which establishes the values of the three independent volume-averaged variables at the next increment in time. In the case of this model and with references to the left hand side of Equations 1, 2, and 3, the variables ρ, W, and

$\overline{\rho s}$ are ones for which a solution is sought. Solution is now straightforward and will be illustrated for one variable - the volume-averaged density. Considering that this method is applicable to any volume, the subscript "k", indicating the k-th volume will be dropped. The Taylor series for volume-averaged density correct to second order can be written as:

$$\bar{\rho}(t+\Delta t) = \bar{\rho}(t) + \frac{\partial \bar{\rho}(t)}{\partial t} \Delta t + \frac{\partial^2 \bar{\rho}(t)}{\partial t^2} \frac{(\Delta t)^2}{2} \tag{16}$$

where:

$\bar{\rho}(t)$ is established by the initial conditions or from the previous time step.

$\frac{\partial \bar{\rho}(t)}{\partial t} = \frac{1}{V} (W_i - W_{i+1})$ from Equation 1 and differentiating this equation with respect to time yields:

$$\frac{\partial^2 \bar{\rho}(t)}{\partial t^2} = \frac{1}{V} \left(\frac{\partial W_i}{\partial t} - \frac{\partial W_{i+1}}{\partial t} \right) \tag{17}$$

Examination of Equation 17 reveals that the right-hand side is composed of derivatives of station values of flow with respect to time. Since Equation 2 will supply only the derivatives of the volume-averaged flow with respect to time, use of an interpolation scheme for obtaining station values from volume-averaged values will permit Equation 17 to be solved for the second partial derivative of volume-averaged density with respect to time. Equations 1 and 17 then can be substituted into Equation 16 to obtain the estimate of the volume averaged density correct to second order at the next increment in time. Equation 17 implies that first derivatives with respect to time of a large number of terms (e.g., F_B, P_M, and S_F) will be required. Although these expansions are lengthy, they can be derived in a straightforward manner and will not be reproduced here. Similarly, this technique can be used for the remaining two variables ($\bar{W}$ and $\overline{\rho s}$) and can be continued from one time step to the next for the desired number of time steps.

3.2 DESCRIPTION OF STABILITY ANALYSIS TECHNIQUE

The following paragraphs explain the methods which are employed in the present study to determine the stability of the compression system model at various steady-state operating points on a speed line. First, let us rewrite Equations 1 and 2 using a slightly different notation and Equation 3 by expanding the left-hand side and substituting Equation 1 as follows:

$$\dot{\rho}_k = \frac{1}{V_k} (W_i - W_{i+1}) \tag{18}$$

$$\dot{W}_k \quad \frac{g_o}{L_k} \left[\frac{W_i C_{z_i}}{g_o} - \frac{W_{i+1} C_{z_{i+1}}}{g_o} + P_i A_i - P_{i+1} A_{i+1} \right. \tag{19}$$

$$\left. - P_m (A_i - A_{i+1}) + F_B \right]$$

$$\dot{s}_k = \frac{1}{\rho_k V_k} \left[W_i s_i - W_{i+1} s_{i+1} + S_F - \bar{s}_k W_i + \bar{s}_k W_{i+1} \right] \tag{20}$$

If we choose ρ_k, W_k, and s_k, (volume averaged properties) to be state variables, then the nonlinear Equations 18 through 20 can be written in the general form

$$\dot{\underline{X}} = f(\underline{X}) \tag{21}$$

where $\underline{X}$ is an n vector composed of state variables and $f(\underline{X})$ is a continuously differentiable n vector. In the case of one general volume, the k-th, Equation 21 would take the form of Equations 22 through 24 where the right hand sides of Equations 18 through 20 have been shown functionally in terms of the applicable state variables.

$$\dot{\rho}_k = f_1 (\bar{\rho}_{k-2}, \bar{W}_{k-2}, \bar{s}_{k-2}, \bar{\rho}_{k-1}, \bar{W}_{k-1}, \bar{s}_{k-1}, \bar{\rho}_k, \bar{W}_k, \bar{s}_k, \bar{\rho}_{k+1}, \bar{W}_{k+1}, \bar{s}_{k+1}) \tag{22}$$

$$\dot{W}_k = f_2 (\bar{\rho}_{k-2}, \bar{W}_{k-2}, \bar{s}_{k-2}, \bar{\rho}_{k-1}, \bar{W}_{k-1}, \bar{s}_{k-1}, \bar{\rho}_k, \bar{W}_k, \bar{s}_k, \bar{\rho}_{k+1}, \bar{W}_{k+1}, \bar{s}_{k+1}) \tag{23}$$

$$\dot{s}_k = f_3 (\bar{\rho}_{k-2}, \bar{W}_{k-2}, \bar{s}_{k-2}, \bar{\rho}_{k-1}, \bar{W}_{k-1}, \bar{s}_{k-1}, \bar{\rho}_k, \bar{W}_k, \bar{s}_k, \bar{\rho}_{k+1}, \bar{W}_{k+1}, \bar{s}_{k+1}) \tag{24}$$

It is noted that the above representation is applicable to either bladed or free volumes and may require state variable information from two upstream volumes and one downstream volume. The state variables from the adjacent upstream volume and the adjacent downstream volume are required because of the interpolation technique which is employed. The second upstream volume is required since stator exit conditions are functions of the rotor incidence angle. In general, not all state variables as indicated by Equations 22

through 24 will be required. For a compression system represented by k volumes we can write the system of equations in the following general form noting that the time derivatives will not be functions of all the system state variables.

$$\begin{bmatrix} \dot{\bar{\rho}}_1 \\ \dot{\bar{W}}_1 \\ \dot{\bar{s}}_1 \\ \dot{\bar{\rho}}_2 \\ \dot{\bar{W}}_2 \\ \dot{\bar{s}}_2 \\ \cdot \\ \cdot \\ \cdot \\ \cdot \\ \cdot \\ \dot{\bar{\rho}}_k \\ \dot{\bar{W}}_k \\ \dot{\bar{s}}_k \end{bmatrix} = \begin{bmatrix} f_1(\bar{\rho}_1,\bar{W}_1,\bar{s}_1,\bar{\rho}_2,\bar{W}_2,\bar{s}_2, \text{--------}\bar{\rho}_k,\bar{W}_k,\bar{s}_k) \\ f_2(\bar{\rho}_1,\bar{W}_1,\bar{s}_1,\bar{\rho}_2,\bar{W}_2,\bar{s}_2, \text{--------}\bar{\rho}_k,\bar{W}_k,\bar{s}_k) \\ f_3(\bar{\rho}_1,\bar{W}_1,\bar{s}_1,\bar{\rho}_2,\bar{W}_2,\bar{s}_2, \text{-------}\bar{\rho}_k,\bar{W}_k,\bar{s}_k) \\ \cdot \\ \cdot \\ \cdot \\ \cdot \\ \cdot \\ \cdot \\ \cdot \\ \cdot \\ f_{3k-1}(\bar{\rho}_1,\bar{W}_1,\bar{s}_1,\bar{\rho}_2,\bar{W}_2,\bar{s}_2\text{-------}\bar{\rho}_k,\bar{W}_k,\bar{s}_k) \\ f_{3k}(\bar{\rho}_1,\bar{W}_1,\bar{s}_1,\bar{\rho}_2,\bar{W}_2,\bar{s}_2, \text{-------}\bar{\rho}_k,\bar{W}_k,\bar{s}_k) \end{bmatrix} \tag{25}$$

Keeping in mind the notation of Equation 25, we return to the more simple notation of Equation 21. Now let us expand the nonlinear system of functions implied by Equation 21 about an equilibrium (steady-state) operating point on a speed line in a multivariable Taylor's series. A new variable $\underline{Y}=\underline{X}-\underline{X}_e$ is introduced which shifts the origin to the equilibrium point. At this point the higher order terms are neglected and Equation 21 becomes

$$\dot{\underline{Y}} = \underline{A}\,\underline{Y} \tag{26}$$

where $\underline{A}$ is a 3k × 3k matrix known as the Jacobian matrix. The $\underline{A}$ matrix can be written as

$$\underline{A} = \begin{bmatrix} \frac{\partial f_1}{\partial \rho_1} & \frac{\partial f_1}{\partial W_1} & \frac{\partial f_1}{\partial s_1} & \frac{\partial f_1}{\partial \rho_2} & \frac{\partial f_1}{\partial W_2} & \frac{\partial f_1}{\partial s_2} & \cdots & \frac{\partial f_1}{\partial \rho_k} & \frac{\partial f_1}{\partial W_k} & \frac{\partial f_1}{\partial s_k} \\ \frac{\partial f_2}{\partial \rho_1} & \frac{\partial f_2}{\partial W_1} & \frac{\partial f_2}{\partial s_1} & \frac{\partial f_2}{\partial \rho_2} & \frac{\partial f_2}{\partial W_2} & \frac{\partial f_2}{\partial s_2} & \cdots & & & \\ \vdots & & & & & & & & & \\ \frac{\partial f_{3k}}{\partial \rho_1} & \frac{\partial f_{3k}}{\partial W_1} & \frac{\partial f_{3k}}{\partial s_1} & \cdots & & & & \frac{\partial f_{3k}}{\partial \rho_k} & \frac{\partial f_{3k}}{\partial W_k} & \frac{\partial f_{3k}}{\partial s_k} \end{bmatrix} \quad (27)$$

The formulation of the $\underline{A}$ matrix elements is described in Appendix A.

The stability of the system of equations can be determined according to the first method of Liapunov (Reference 7) who showed that if the eigenvalues of the $\underline{A}$ matrix have nonzero real parts, then the stability of the nonlinear system of equations at the equilibrium point $\underline{X}_e$ is the same as that of the linear system of equations at $\underline{Y} = 0$. Therefore, if all the eigenvalues of the characteristic equation of the $\underline{A}$ matrix have negative real parts, then the equilibrium point $\underline{X}_e$ is asymptotically stable.

Since only the sign of the real part of the roots (eigenvalue) is important to the stability of the system of equations, significant reduction in computation time can be gained by determining only the sign of the roots rather than determining the values of the roots themselves. The stability

and frequency response analysis techniques employed during the clean-inlet-flow studies, where an 87 × 87 $\underline{A}$ matrix was being examined, were based on the work of Seidel (Reference 8). The characteristic equation of the $\underline{A}$ matrix is obtained by the method of Danilevsky (Reference 9) which reduces the matrix to Frobenius form. Then the signs of the roots of the characteristic equation are found by the alternate Routh-Hurwitz formulation method (Reference 10). Although the Routh, Hurwitz, and the alternate Routh-Hurwitz formulation methods for determining the signs of the roots are all equivalent, the details of the calculational procedures are different and offer varying degrees of computational simplicity. However, according to Routh, stability is insured if all the coefficients of the characteristic equation are present and positive (necessary condition) and that all the terms in the first column of the Routh array (Reference 7) are positive (sufficient condition).

Much technical effort was expended during the early stages of this program in developing techniques to avoid computational underflow and overflow problems which were experienced when analyzing the 87 × 87 Jacobian matrix for system stability. Two precautionary measures were undertaken to avoid these numerical problems which inevitably occur for models with numerous volumes. A unit length scale factor was imposed to optimize the range of matrix elements by keeping the elements as small as possible. This scale factor scaled all units of length in the $\underline{A}$ matrix and resulted in a span of values from 10^0 through 10^5 (versus 10^{-2} through 10^{11} prior to scaling). An overall scale factor was then applied to the matrix, positioning the range as equally as possible about unity, i.e., $(10^{-3} - 10^2)$. This further reduces the chances of computational problems by numerically balancing the matrix.

Problems were encountered with the Reference 8 methods during the distorted-inlet-flow studies where a 153 × 153 $\underline{A}$ matrix was involved even though double precision arithmetic was employed. Considerable light was shed on the problems by Wilkinson (Reference 11). "In general, the reduction to Frobeius form (or the computation of the characteristic equation) is much less satisfactory than the reduction to tri-diagonal form. For many quite harmless looking distributions of eigenvalues the Frobenius form is extremely ill-conditioned, and it is common for double precision arithmetic to be quite inadequate." Upon investigation it was found that the Aircraft Engine Group of General Electric had purchased a subroutine package* that would circumvent these problems and would only require single precision arithmetic since, in this case, the roots are found directly by reducing the $\underline{A}$ matrix to Hessenberg form (Reference 11). This subroutine package was used throughout the distorted-inlet-flow studies.

---

*Interpretational, Mathematical and Statistical Library-IMSL
Interpretational, Mathematical and Statistical Libraries, Inc.
Bellaire
Houston, Texas 77036

3.3 DESCRIPTION OF FREQUENCY RESPONSE ANALYSIS TECHNIQUE

The frequency response analysis technique of Reference 8 was employed in this study and is essentially a Laplace transfer function analysis of a set of linearized equations.

$$\dot{\underline{Y}} = \underline{A}\,\underline{Y} + \underline{B}\,\underline{U} \tag{28}$$

$$\underline{R} = \underline{C}\,\underline{Y} \tag{29}$$

These equations describe 1) the response of the state variables at the equilibrium operating point to input forcing functions and 2) the output response in terms of a linear combination of the other variables.

The homogeneous linearized system of equations describing the compressor determines the $3k \times 3k$ matrix and is described in Section 3.2 (Equation 26). The state variable fector, $\underline{Y}$ is a $3k \times 1$ vector. $\underline{U}$ is a $n \times 1$ vector input forcing function and $\underline{B}$ is a $3k \times n$ matrix of the form:

$$\underline{B} = \begin{bmatrix} \frac{\partial f_1}{\partial u_1} & \frac{\partial f_1}{\partial u_2} & \cdots & \frac{\partial f_1}{\partial u_n} \\ \frac{\partial f_2}{\partial u_1} & & & \frac{\partial f_2}{\partial u_n} \\ \vdots & & & \\ \frac{\partial f_{3k}}{\partial u_1} & & & \frac{\partial f_{3k}}{\partial u_n} \end{bmatrix} \tag{30}$$

The partial derivatives used to form the $\underline{B}$ matrix are given in Appendix B. $\underline{R}$ is a $m \times 1$ output vector and $\underline{C}$ is a $m \times 3k$ matrix expressing the linear relationship between the state variables and the output variables.

The Laplace Transform equivalents of the system equations represented by Equations 28 and 29 are

$$s\,\underline{Y}(s) = \underline{A}\,\underline{Y}(s) + \underline{B}\,\underline{U}(s) \tag{31}$$

$$\underline{R}(s) = \underline{C}\,\underline{Y}(s) \tag{32}$$

where s is the Laplace variable. Equations 31 and 32 can be written in transfer function form as

$$\frac{\underline{R}(s)}{\underline{U}(s)} = \underline{C}\,(s\,\underline{I} - \underline{A})^{-1}\,\underline{B} \tag{33}$$

where $\underline{I}$ is the identity matrix. As it stands, Equation 33 requires a matrix inversion with a free parameter and is not compatible with digital computer calculations. The solution is readily obtained, however, for any one or all elements of the matrix transfer function.

For example the transfer function between the k-th element of $\underline{R}$ and the l-th element of $\underline{U}$ is

$$\frac{\mathcal{L}\{\underline{R}\}_k}{\mathcal{L}\{\underline{U}\}_\ell} = \frac{\det\,(\underline{W})}{\det\,(s\,\underline{I} - \underline{A})} \tag{34}$$

where $\underline{W}$ is an appropriate system Wronskian matrix. Details are given in Appendix C.

Upon expansion, the numerator and denominator of the transfer function represented by Equation 32 are each polynomials in s. Using one of the subroutines in Reference 8, the transfer function frequency response is numerically evaluated by substituting $s = j\omega$ where ω is a given frequency and j is the imaginary number $\sqrt{-1}$.

3.4 DESCRIPTION OF J85-13 COMPRESSOR MODEL

The previously discussed stability analysis and frequency response techniques were used to study the characteristics of the J85-13 turbojet engine. The compressor of a J85-13 engine has eight stages with a variable camber IGV and variable third, fourth, and fifth stage bleeds located in each stator channel at the casing wall. The IGV trailing edge flaps and the bleeds are ganged together and are scheduled as a function of corrected speed biased by compressor-face total temperature. A cross-section view of the J85-13 engine in the compressor and combustor regions is shown in Figure 1. The nominal IGV and bleed schedules for the bill of material engine are given in Figure 2.

It is appropriate to discuss the two engines modeled in this study. The pure total-pressure distortion patterns that were simulated during this study were obtained during testing of a J85-13 engine known as the "Moss" engine (Reference 12). This engine was run in support of the NASA casing treatment program. The clean inlet and distortion data utilized in this model were obtained from the untreated configuration with solid compressor-case inserts. It should be noted that this engine tends to be representative

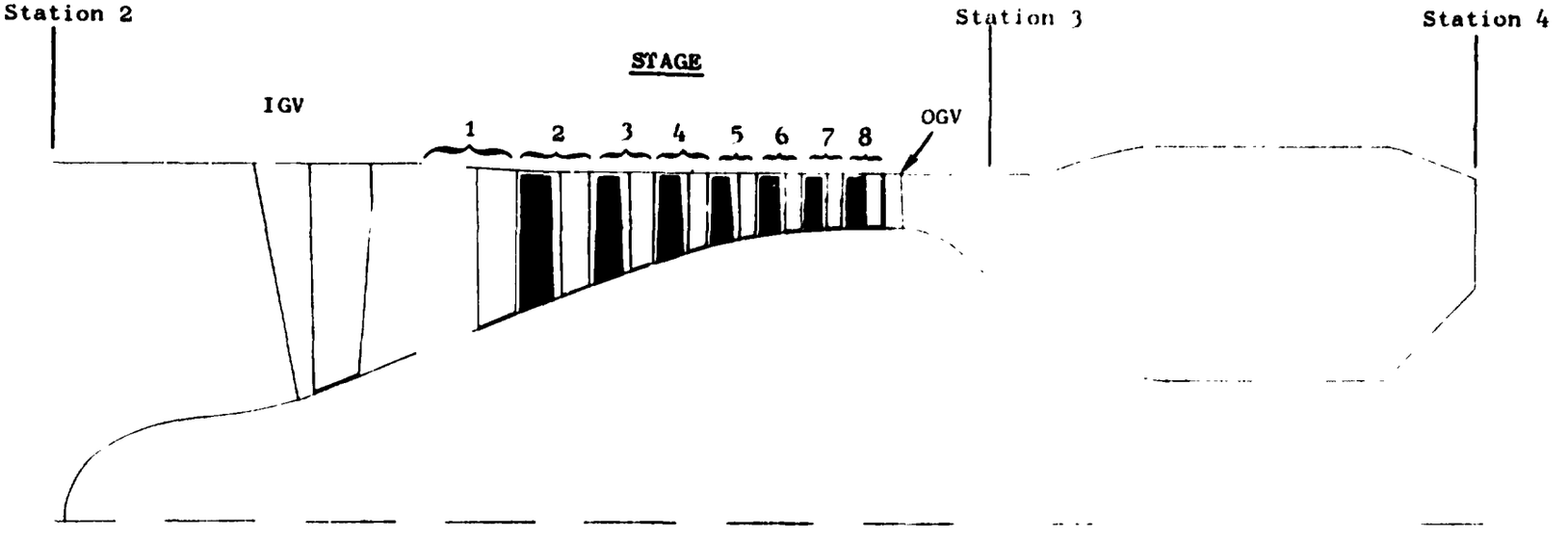

Figure 1. Section View of J85-13 Compressor.

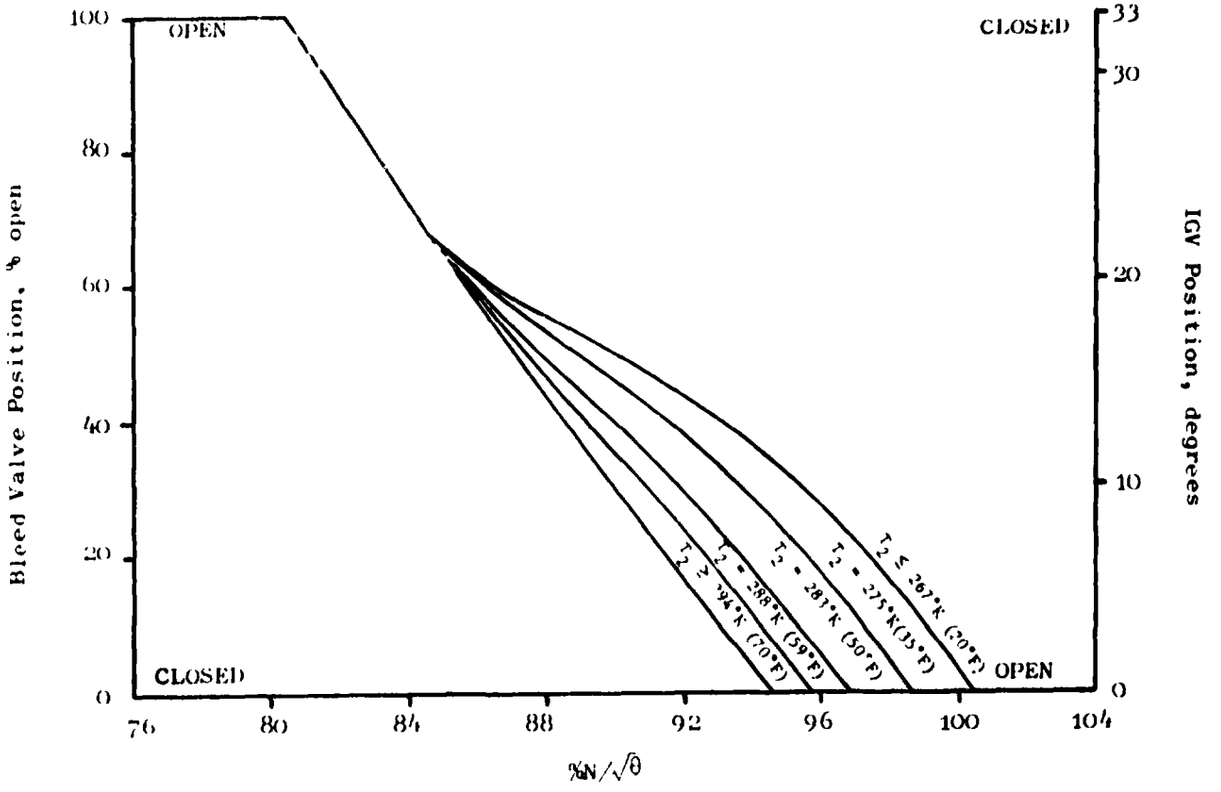

Figure 2. Nominal IGV And Bleed Valve Schedule For Bill Of Material Engine.

of a deteriorated engine. For comparative purposes, clean inlet flow studies were also made on a J85-13 engine known as the "Mehalic" engine (Reference 13). NASA had used this engine to obtain pure total-temperature distortion pattern data and the combined total-pressure and total-temperature distortion pattern data.

For the purposes of this study, the compressor model includes volumes upstream of the IGV to the distortion measurement plane and downstream of the OGV continuing to a choke plane located at the turbine nozzle diaphragm (A_4). The purpose of including these extra volumes is to insure that realistic boundary conditions can be imposed.

The compressor model consists of twenty-nine volumes. There are 18 bladed volumes (one blade row per volume) consisting of the IGV, rotors 1-8, stators 1-8, and the OGV and 11 free volumes. These free volumes consist of two volumes between the instrumentation plane and the leading edge of the IGV, a volume between the trailing edge of the IGV and the leading edge of rotor 1, and eight volumes between the trailing edge of the OGV and the turbine diaphragm. This configuration is shown schematically in Figure 3. It should be noted that the length of a rotor blade row extends from the trailing edge of the upstream stator to the leading edge of the downstream stator and includes the axial inter-blade row gaps while the length of a stator blade row extends from the leading edge of the stator to the trailing edge of the stator. For further geometrical details, the reader is referred to Reference 3.

The blade work on the fluid is accomplished in a distributed, but unspecified, manner across a rotor volume length. All losses are assumed to take place in rotors, that is, no losses are accounted for in blade free volumes or stator blade volumes. However, this is not a restriction of the model. The rotor deviation angles vary as functions of the incidence angle.

At this point, it is worth mentioning that because a blade row formulation is being used, stage characteristics information was used in the form of a relative total-pressure loss coefficient and a deviation angle rather than the more often used non-dimensional work and pressure coefficients as a function of flow coefficient. This approach tends to decouple the inlet and exit stations of a blade row in a dynamic analysis since volume storage of mass, momentum, and energy are permitted within the work producing volume. Further, splitting a stage volume into two blade row volumes will potentially double the frequency capabilities of a dynamic compression component model. The relative total-pressure loss coefficients and the deviation angles that were used during this study are given in both graphical and polynomial form in Reference 3.

The third, fourth, and fifth stage bleed flows in the model are removed at the exit of the stator while holding exit air angle constant. The percentage of inlet flow that is removed from each stage is given in Table 1.

Figure 3. Schematic Of Model Volumes.

Table 1. Bleed Removal Schedule (Percent of Inlet Physical Flow).

Engine	Corrected Speed	Stage 3	Stage 4	Stage 5
Moss	80	3.95%	4.90%	5.78%
Moss	87	2.28	2.83	3.33
Moss	94	0	0	0
Moss	100	0	0	0
Mehalic	87	1.20	1.49	1.76
Mehalic	94	0	0	0
Mehalic	100	0	0	0

During NASA testing of the Moss and Mehalic engines, the T_{T_2} control bias as shown in Figure 2 was subverted. The Moss engine was controlled to 294.3° K (70° F) or higher temperature curve and the Mehalic engine had a modified schedule. Further details are given in Reference 3.

The boundary conditions imposed upon the model consist of specifying the total pressure and total temperature entering volume 1 and specifying the value of the exit flow function ($W\sqrt{T_s}/P_s$) at the exit of the last volume.

4.0 RESULTS

The results of the clean-inlet-flow, frequency-response, and distorted inlet-flow analyses of the J85-13 compression system are presented in this section. The clean-inlet-flow stability analyses were conducted using the Routh-Hurwitz stability criterion, that is, only the signs of the roots of the characteristic equation were examined. The frequency response of the compressor was determined by evaluating the Laplace transfer function of the linearized system of equations. The distorted-inlet-flow stability analyses were accomplished by first constructing a parallel compressor model and then conducting the stability analyses by actually determining the roots (eigenvalues) of the characteristic equation. The signs of the real parts of the roots were examined (all negative values for stability) to determine if the operating condition was stable.

4.1 CLEAN-INLET-FLOW SURGE LINE ANALYSES

The first step in verifying the state equations in their linearized form was accomplished by duplicating the J85-13 clean-inlet-flow compressor map. Figure 4 provides a detailed view of the stability analysis process for the 80% corrected speed line. These linearized analyses (L-A) results are compared to the results of the time-dependent (T-D) dynamic analysis program (Reference 3) and to engine test data (Reference 13). The Routh-Hurwitz stability analysis technique was used to verify the stability for five surge-free conditions on the speed line and to predict the surge point within a weight flow uncertainty of ±0.05 kg/sec (±0.11 lbm/sec). Figure 5 shows the clean-inlet-flow compressor map for the J85-13 "Moss" engine. The 80, 87, 94, and 100 percent corrected speeds are shown extending over a range of pressure ratios from surge to the region of the nominal sea-level-static operating line.

At 94 percent corrected speed, the linearized analysis failed to match the surge point. At this point it was appropriate to question whether this failure is a result of a limitation of the linearized blade row model or is the result of some minor error in the Jacobian matrix formulation which had not been discovered. In an effort to determine the reasons for this failure, two areas of concern were investigated: 1) the formulation of the $\underline{A}$ matrix elements and 2) the blade characteristics input (loss coefficients, deviation angles, and lift direction correction angles) for the Moss engine 94 percent corrected speed line. The $\underline{A}$ matrix elements were independently rederived and to our best knowledge are error free. Further, as explained in the next section (Section 4.2) it was possible to obtain an independent assessment of the accuracy of the formulation by comparing the frequency responses of the state variables ρ, W, and s at selected stations with the time-dependent solutions. This assessment showed that close agreement could be obtained between the linearized analysis and time-dependent-solution state variables. In the process of making minor changes or revisions to the $\underline{A}$

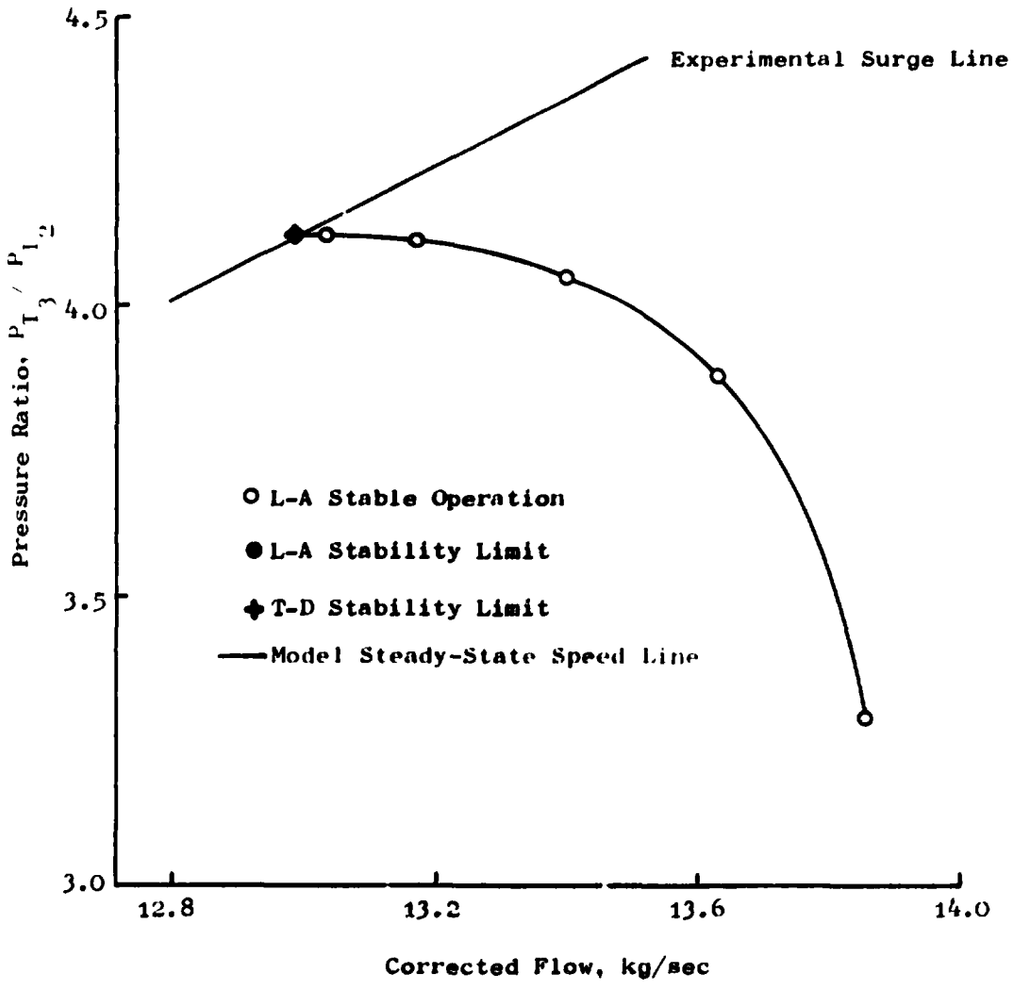

Figure 4. Detailed View of "Moss" Engine 80% Corrected Speed Line Stability Analysis.

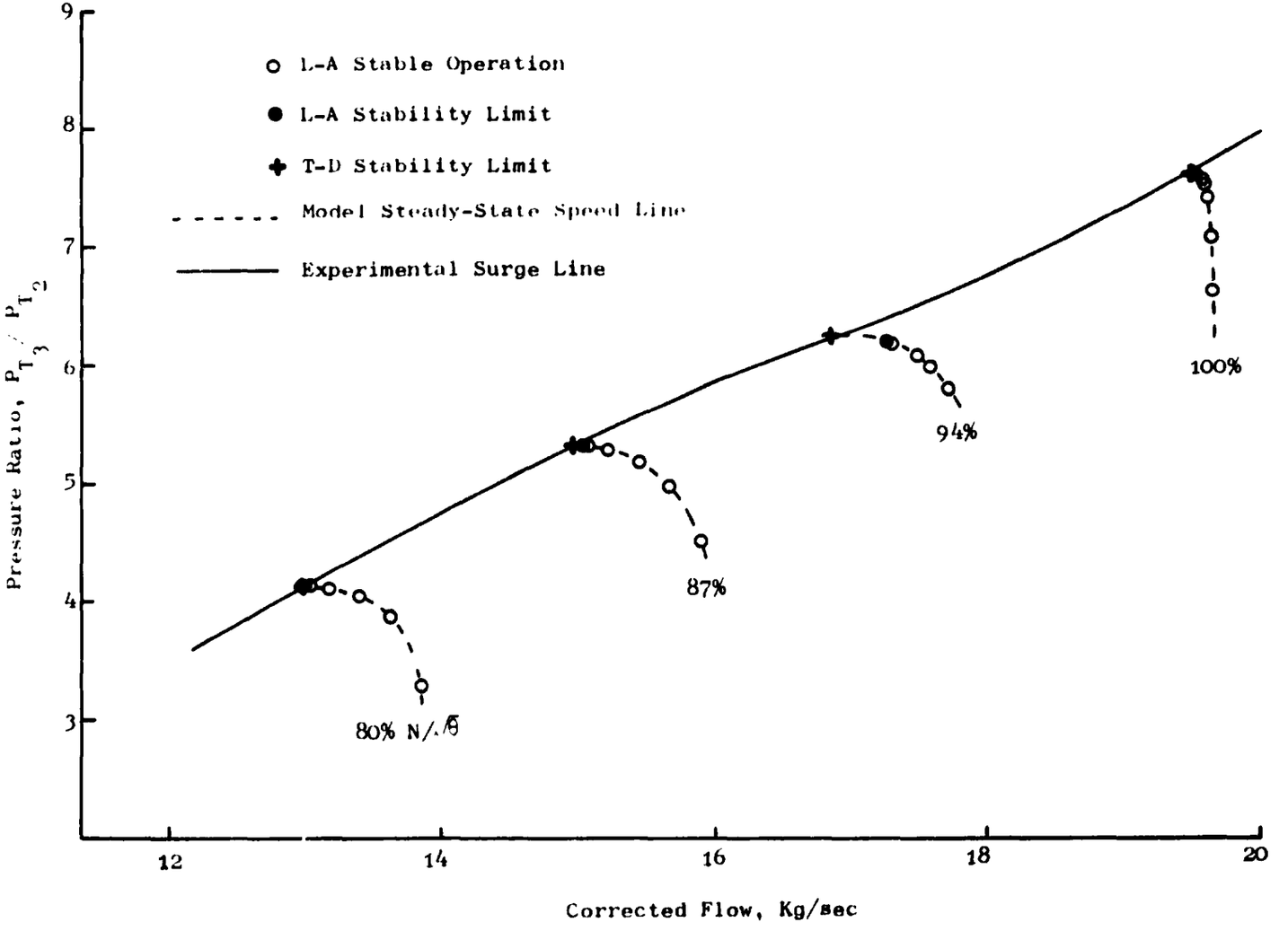

Figure 5. "Moss" Engine Stability Analyses Results.

matrix, it was noticed that the location of the 94 percent corrected speed instability point would move significantly although the location of the stability points of the 80, 87, and 100 percent corrected speed lines moved almost imperceptibly. At this juncture it was questioned whether the blade row characteristics might play a part in this sensitivity. The pressure coefficients Ψ' (in part from which the blade row characteristics are derived) for each stage of the Moss engine were examined as a function of flow coefficient. As can be seen from examination of Figure 6 (taken from Reference 3), Stages 2, 3, and 4 are operating on the positive slope portion of their characteristic at instability (lowest shown flow coefficient). Another J85-13 engine known as the Mehalic engine had been modeled at 94 percent corrected speed during the Reference 3 study. Examination of the pressure coefficient - flow coefficient relationships for this compressor as depicted in Figure 7 reveals that only two stages are operating on the positive slope portion of their characteristics at instability. It should be noted that in general, the fewer the number of stages operating on positive slope characteristics, the more stable the compressor. The Mehalic engine clean-inlet-flow characteristics were analyzed using the same linearized technique as applied to the Moss engine. The results are shown in Figure 8 and indicate good agreement with test data and the time-dependent model. One can question as to whether the "Moss" engine 94 percent corrected speed stage characteristics are realistic representations of the engine. Since these characteristics were used in the time-dependent model to obtain an accurate prediction of the surge line, it is assumed that there is nothing inherently wrong with these characteristics. Thus, there appears to be no basic error in the formulation of the linearized model, but there does appear to be a sensitivity to the number of stages operating on the positive slope of their characteristics.

These lines of investigation have provided insight, but not the reason for the linearized analysis to inaccurately predict the point of instability for the Moss engine at 94 percent corrected speed. It is suspected that the reason for this discrepancy involves two factors: 1) some of the assumptions employed to permit linearizing the time-dependent model or some minor undiscovered error in an $\underline{A}$ matrix element(s) act to subtly decouple the stages and 2) the number of stages which operate on the positive slope portion of their characteristics. Thus, these two factors acting in concert tend to create a situation which is less stable than should be anticipated.

During the checkout phase when it was necessary to verify the accuracy of the derivation of the $\underline{A}$ matrix elements, it was found that the lack of output information which could be compared with an independent solution seriously impeded the debugging process. Clean-inlet-flow stability checks in essence provided only "go" or "no go" type of information and did not provide detailed dynamic responses of thermodynamic or flow parameters (state variables) which could be compared to the Reference 3 time-dependent model. However, the frequency response analyses discussed in Section 4.2 provided state variable information at each station within the model. By selectively examining the state variable responses in blade free volumes,

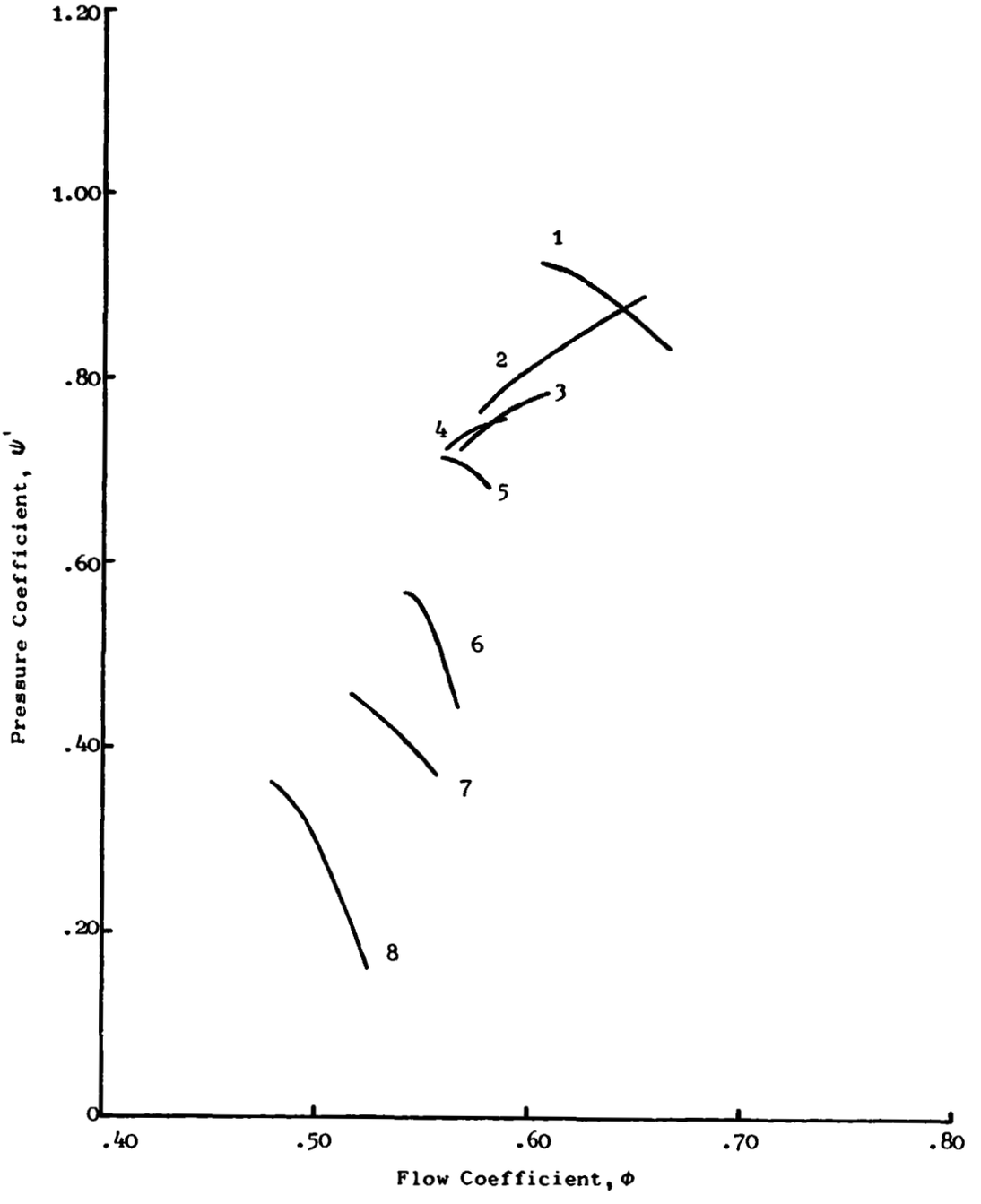

Figure 6. "Moss" Engine Pressure Coefficients, 94% $N/\sqrt{\theta}$.

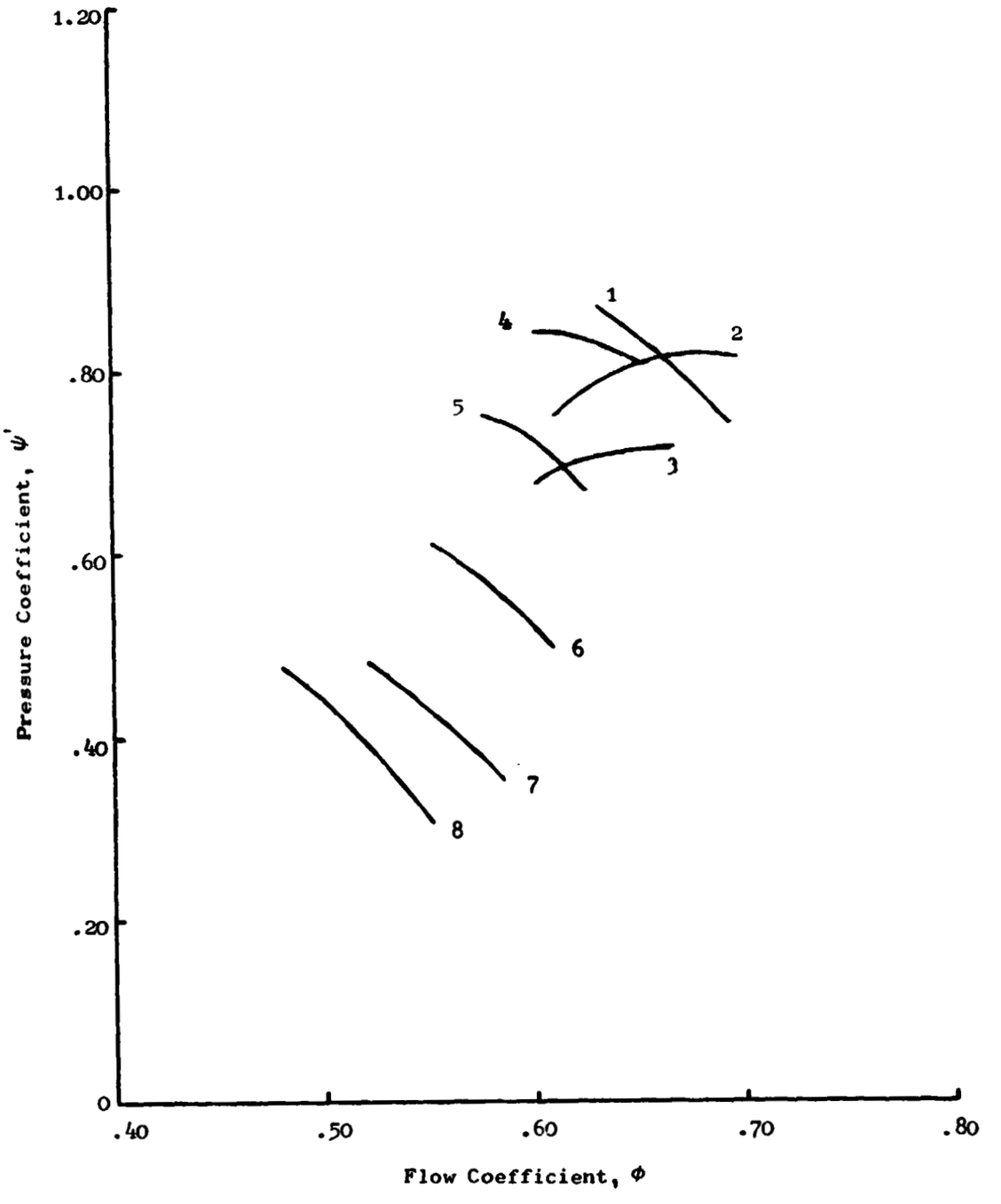

Figure 7. "Mehalic" Engine Pressure Coefficients, 94% $N/\sqrt{\theta}$.

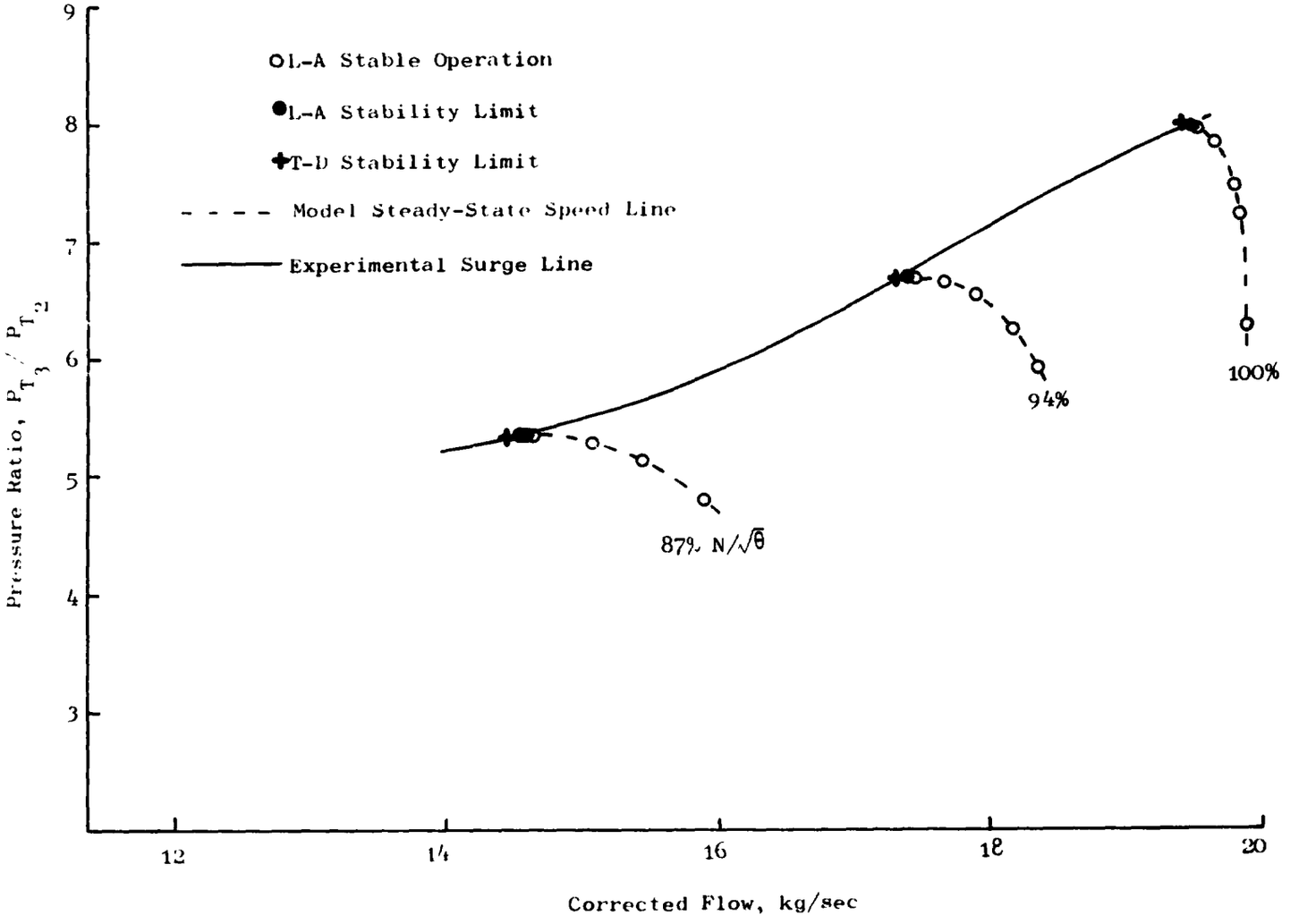

Figure 8. "Mehalic" Engine Stability Analyses Results.

rotor blade row volumes, and stator blade row volumes, and comparing these responses with time-dependent solution results, it was possible to debug the $\underline{A}$ and $\underline{B}$ matrix element formulations in a more efficient and orderly fashion.

For surge line determination alone, the linearized stability analysis method costs are approximately one-fifteenth of those incurred by the time-dependent method of Reference 3.

4.2 FREQUENCY RESPONSE ANALYSIS

The frequency responses of the "Moss" J85-13 compressor were generated using the Jacobian ($\underline{A}$) and input response ($\underline{B}$) matrices and the Reference 8 digital subroutines to determine the Laplace transfer function. The frequency response of compressor-exit state variables ($\bar{p}$, $\bar{W}$, $\bar{s}$) to variations in compressor inlet total pressure and exit flow function over a range of 0.1 to 200 Hz was determined. All investigations were carried out at the 100% corrected speed operating point [PR=6.636, W_c=19.68 kg/sec (93.3 lbm/sec)] for 25 frequencies. The time-dependent program (Reference 3) was run concurrently to provide comparative cases at frequencies of 30, 60, 100, 150, and 200 Hz. Combined plots of amplitude ratio (output to input) and phase angle are given for the range of frequencies investigated. Figures 9 through 11 show the compressor exit state-variable frequency responses to inlet total-pressure oscillations. Good agreement in both amplitude and phase angle is noted between the linearized and dynamic program results. The time-dependent program total-pressure oscillations were ±0.5 percent about the specified inlet pressure. It was found that time-dependent program oscillations of ±3.0 or ±2.0 percent of the inlet total pressure were too large to obtain a match between the time-dependent program and the linearized analyses. Hence, a compression component introduces significant nonlinearities at low amplitudes. Application of the linearized technique for determining planar wave dynamic distortion transfer (Reference 6) must be done with great care since an engine in a highly manueverable aircraft may be subjected to inlet-produced unsteady flows where the amplitudes may be on the order of 10 percent of the inlet mean total pressure.

The amplitude and frequency responses to exit-flow-function oscillations are shown in Figures 12 through 14. The time-dependent program exit-flow-function oscillations were maintained at ±1.0 percent about the mean exit-flow-function value. With this type of boundary condition, it was found that the dynamic program settled out slowly from its "start up" transient. Because it was economically impractical to let every dynamic case completely settle out, some of the minor differences between the linearized and dynamic predictions of the amplitude and frequency responses of the lower frequencies may be attributed to the fact that a stationary state had not been obtained.

A detailed analysis of both the inlet total-pressure and exit-flow-function oscillation cases shows that as 200 Hz is approached a systematic divergence develops between linearized and time-dependent program analyses amplitudes. At this time, no explanation has been found which satisfactorily explains this divergence. It may be that at frequencies equal to or greater

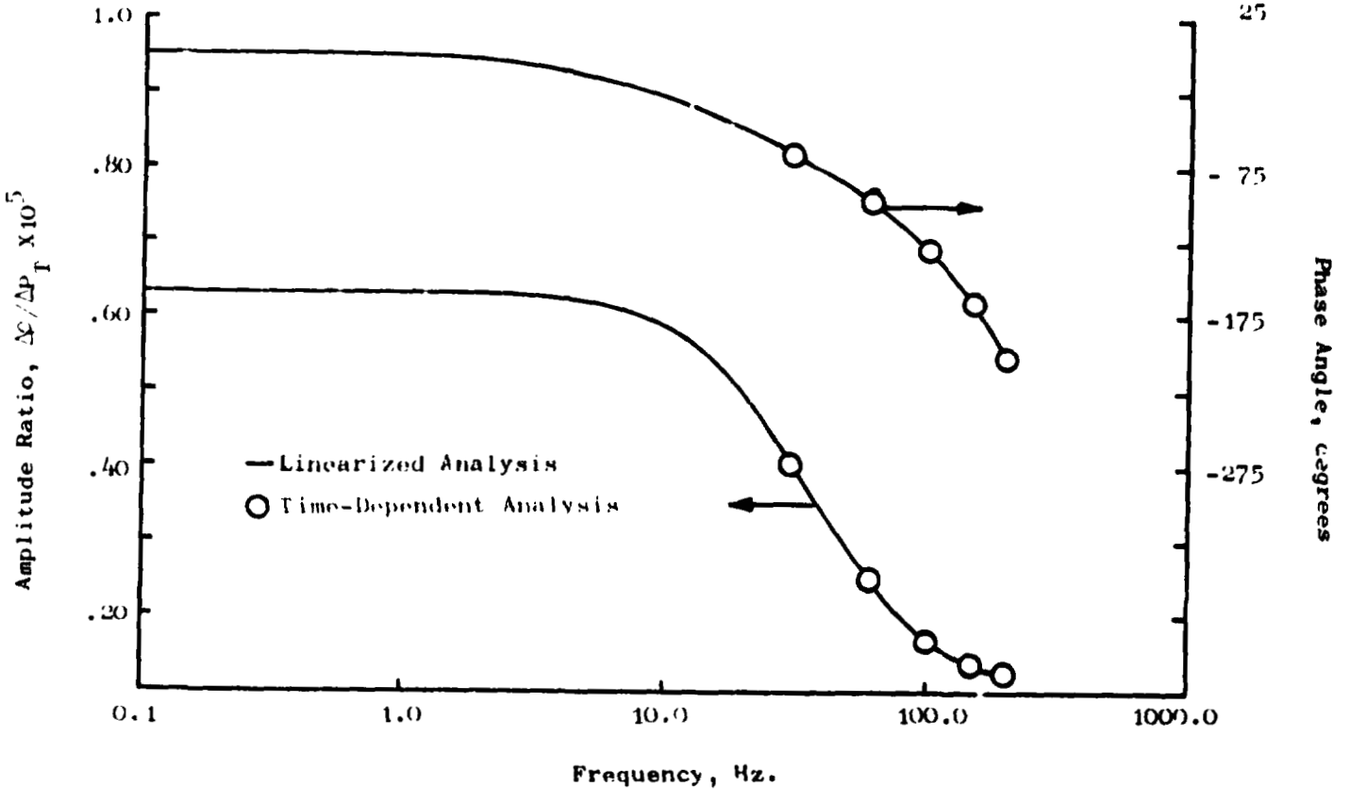

Figure 9. Compressor-Exit-Density Frequency Response to Inlet Total-Pressure Oscillation.

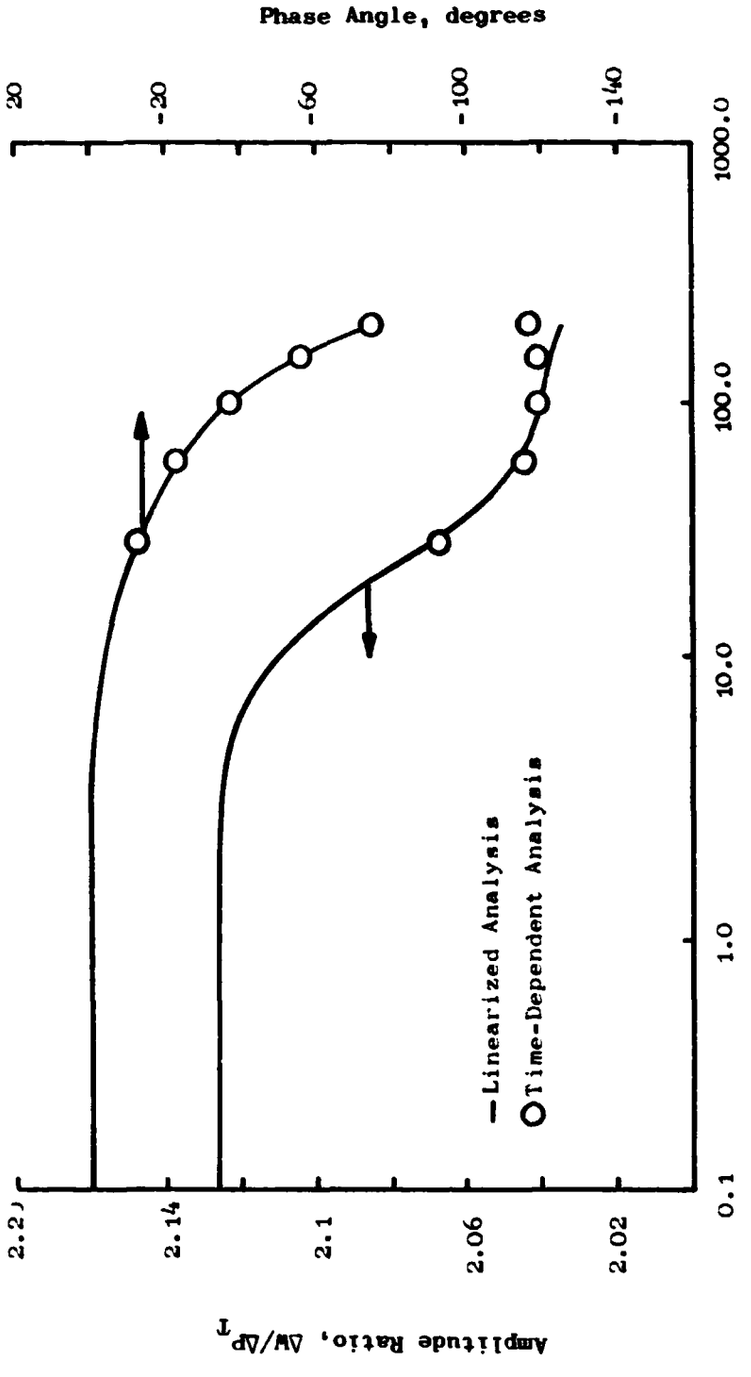

Figure 10. Compressor-Exit-Flow Frequency Response to Inlet Total-Pressure Oscillation.

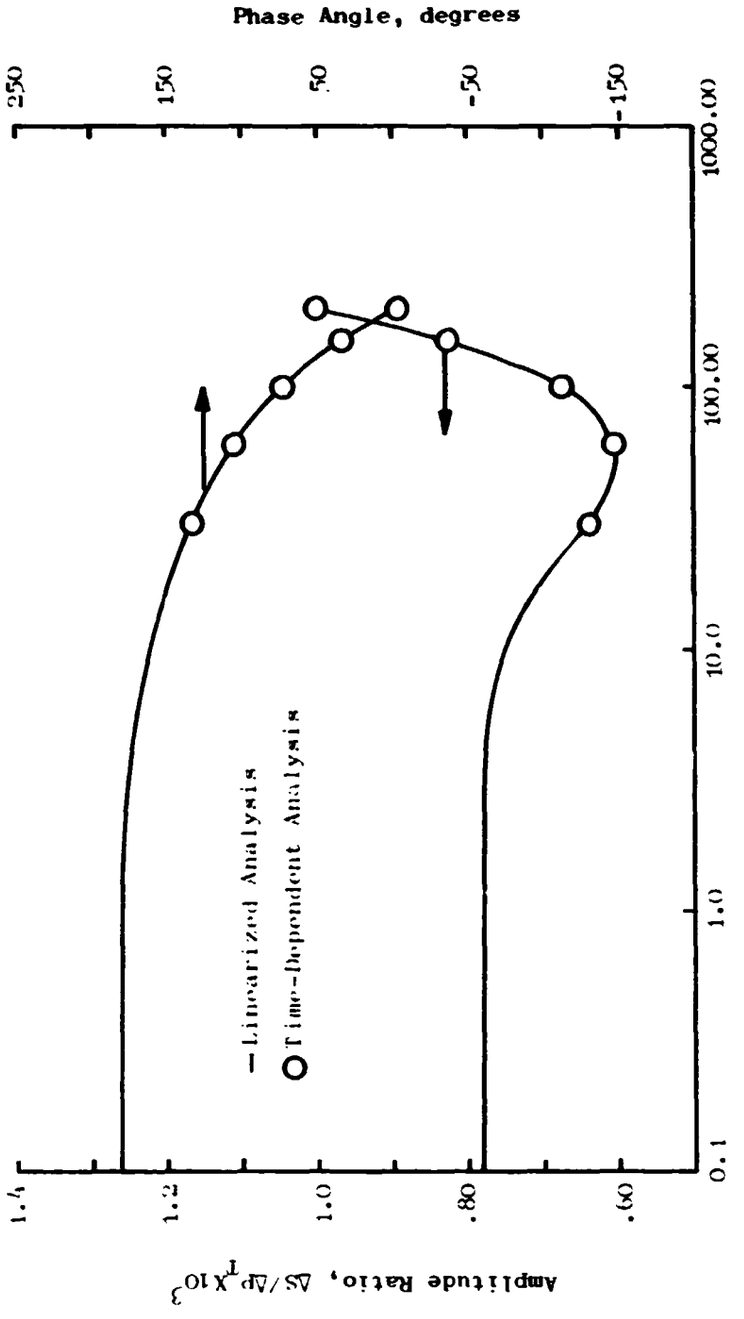

Figure 11. Compressor-Exit-Entropy Frequency Response to Inlet Total-Pressure Oscillation.

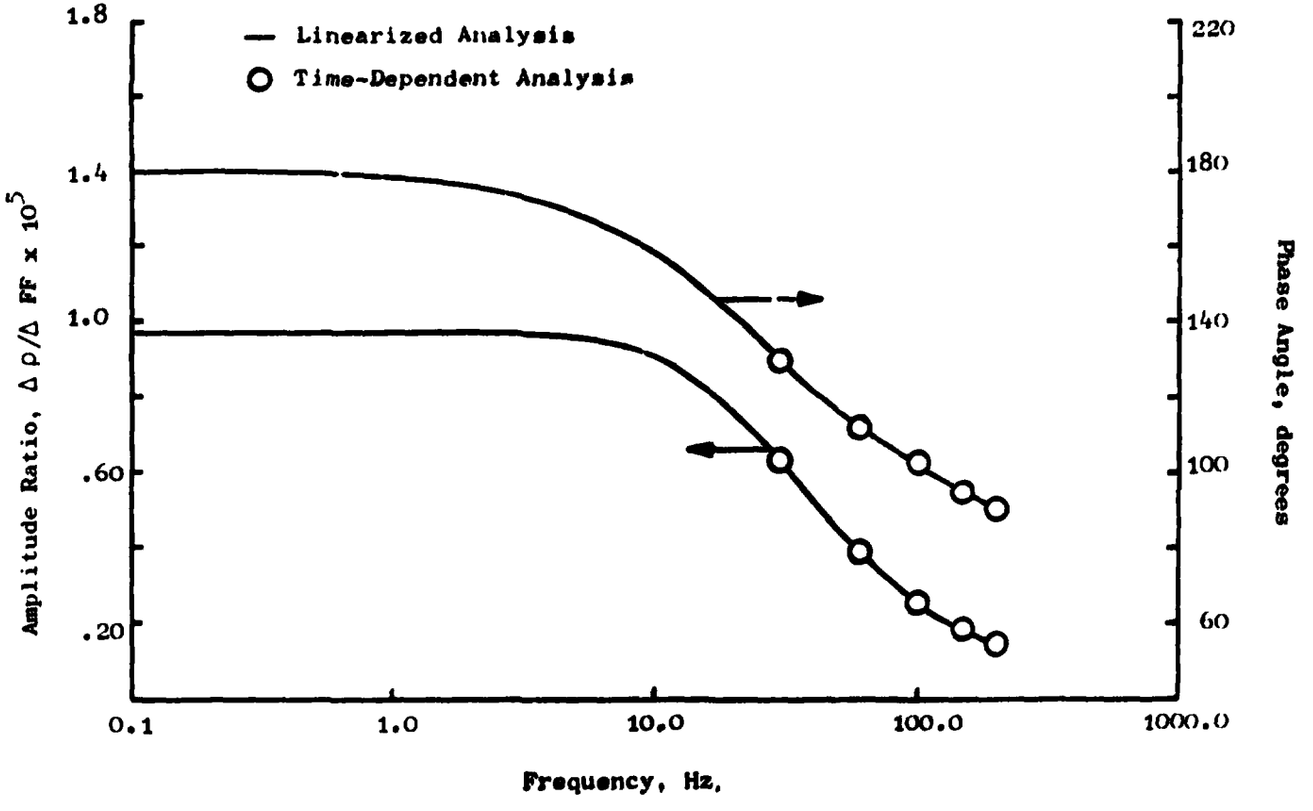

Figure 12. Compressor-Exit-Density Frequency Response to Combustor Exit Flow-Function Oscillation.

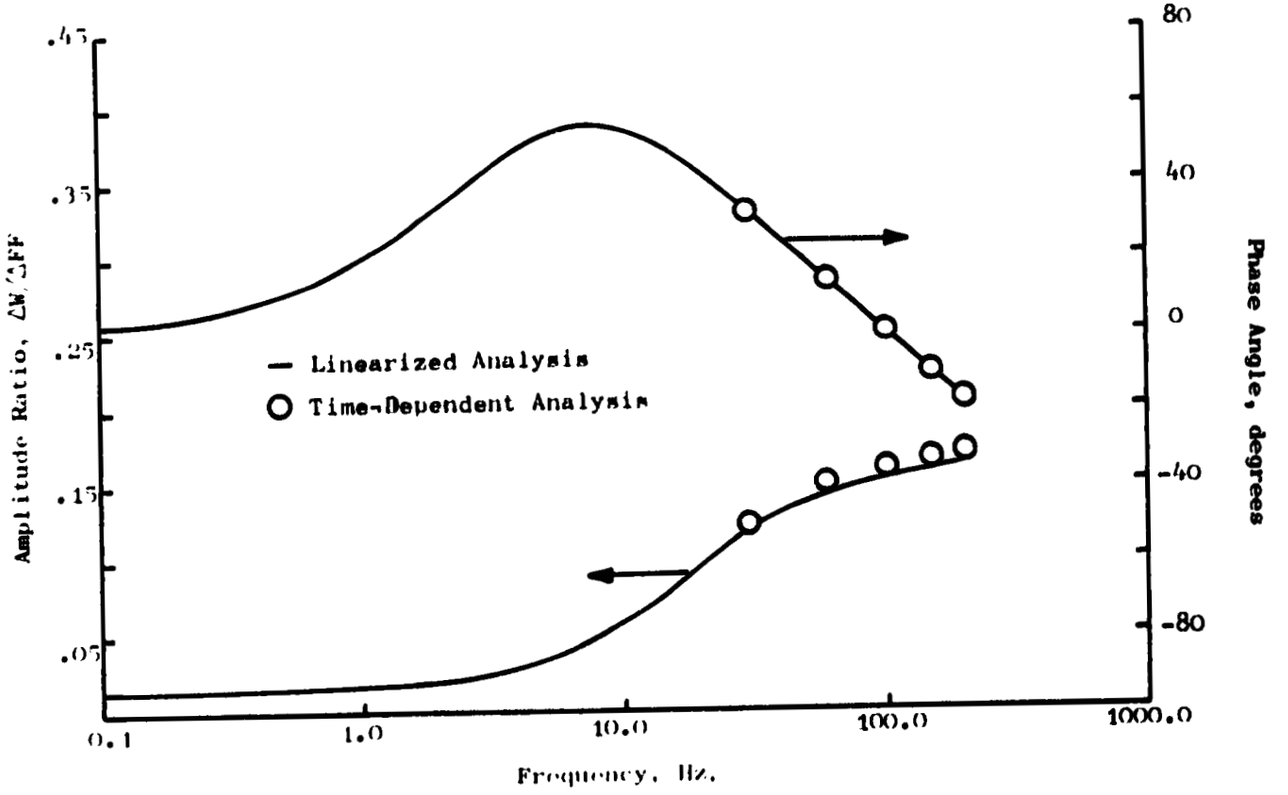

Figure 13. Compressor-Exit-Flow Frequency Response to Combustor Exit Flow-Function Oscillation.

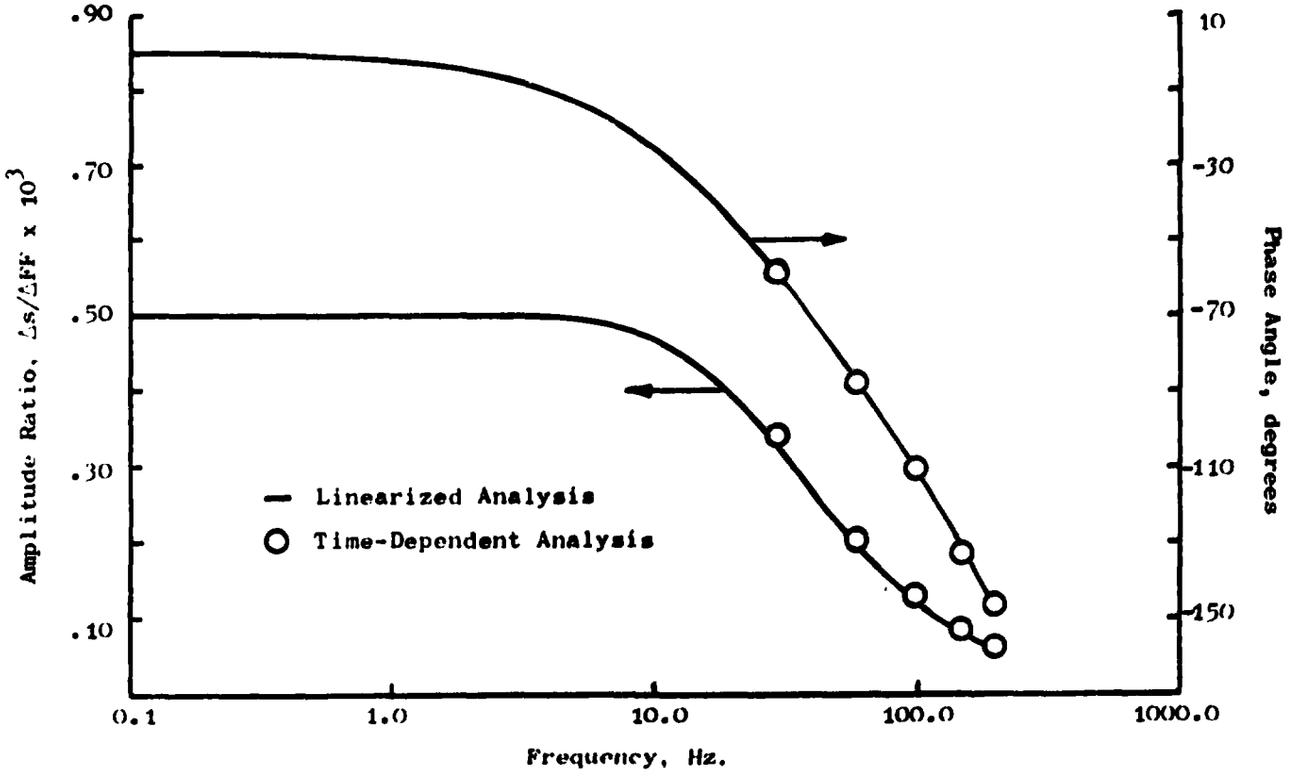

Figure 14. Compressor-Exit-Entropy Frequency Response to Combustor Exit Flow-Function Oscillation.

than 200 Hz for the J85-13 compression system, even though only very small perturbations are being imposed upon the time-dependent model, the nonlinear terms in the macrobalances (Equations 1 through 3) introduce a noticeable contribution to the state variables.

It was concluded that the linearized frequency response and the time-dependent model give essentially equivalent results (in terms of the state variables) in the frequency range of major interest. It is now possible to combine the state variables at the compressor exit to obtain the response of a more easily recognized and measurable quantity, the total pressure. This is accomplished by deriving the functional dependence of the total-pressure fluctuations to the fluctuations of the local state variables. Total derivatives are used to obtain this relationship. Static pressure can be expressed in terms of static density and entropy as:

$$P = P_r \left(\frac{\rho}{\rho_r}\right)^{\gamma} e^{(s-s_r)(\gamma-1)/R} \tag{35}$$

where the subscript "r" denotes reference conditions.

Similarly, Mach number can be expressed in terms of static pressure, static density, and weight flow as

$$M^2 = \frac{W^2}{\rho A^2 \gamma g_o P} \tag{36}$$

Total pressure can be related to static pressure and Mach number at a point by the isentropic relationship

$$P_T = P\left(1 + \frac{\gamma-1}{2} M^2\right)^{\frac{\gamma}{\gamma-1}} \tag{37}$$

The total derivatives of Equations 35, 36, and 37 are respectively:

$$dP = P\left(\frac{\gamma}{\rho} d\rho + \frac{\gamma-1}{R} ds\right) \tag{38}$$

$$dM^2 = \frac{2W\rho P dW - W^2 (\rho dP + P d\rho)}{\rho^2 A^2 \gamma g_o P^2} \tag{39}$$

$$dP_T = \left(1 + \frac{\gamma-1}{2} M^2\right)^{\frac{\gamma}{\gamma-1}} dP + P\left(\frac{\gamma}{2}\right)\left(1 + \frac{\gamma-1}{2} M^2\right)^{\frac{1}{\gamma-1}} dM^2 \tag{40}$$

Substituting Equations 38 and 39 into Equation 40 yields the total-pressure perturbation response characteristics about a steady-state operating point in terms of local state-variable perturbations. In this case, the differentials $d\rho$, dW, and ds represent the frequency response (amplitude and phase) of these state variables in complex form. It is now possible to explicitly calculate the response of compressor-exit total pressure and directly compare the results to those obtained from the time-dependent program. Figures 15 and 16 show this comparison at the 100% corrected speed operating point for inlet total-pressure and exit-flow-function oscillations. Shown in the figures are normalized pressure responses to input normalized inlet total pressure and input normalized exit flow function, respectively. As expected, the compressor attenuates the inlet total-pressure fluctuations. In conclusion, it has been shown that the linearized J85-13 frequency response characteristics match the results obtained from the Dynamic Digital Blade Row Compression Component Stability Model when small amplitude boundary conditions are imposed.

However, it is apparent that for even moderately low amplitudes, the effects of the nonlinear terms as included in the time-dependent model, can cause significant deviation of the time-dependent results from the linearized analysis results. If one were interested in large amplitude planar-wave transfer such as encountered with inlet buzz, then it would be necessary to obtain time-dependent solutions of the nonlinear equations rather than a linearized analysis.

It is important to note that the linearized analysis frequency response technique costs are independent of frequency and in fact, the frequency responses at many frequencies can be obtained for essentially the same cost as one frequency. However, the cost of obtaining frequency responses is directly proportional to the number of stations where the frequency response is desired. On the other hand, the dynamic program is frequency sensitive because of the time to settle out and the period of a given wave. For a given configuration, the costs are independent of the number of frequency responses desired.

It is clear that if the linearized frequency response of a compression component at selected stations is desired, than the linearized technique of this section offers considerable economic advantages. However, if the frequency response of each stage at a given frequency is required, then the dynamic model offers economic advantages for frequencies greater than approximately 20 Hz.

4.3 DISTORTED-INLET-FLOW ANALYSES

The blade-row parallel compressor model of Reference 3 was put in linearized form and resulted in a 153 x 153 matrix for a two sector model. The model was modified to permit flow at a given stage to be removed from the high total-pressure sector at its total pressure and to be reintroduced to the low total-pressure sector at its total pressure assuming that the

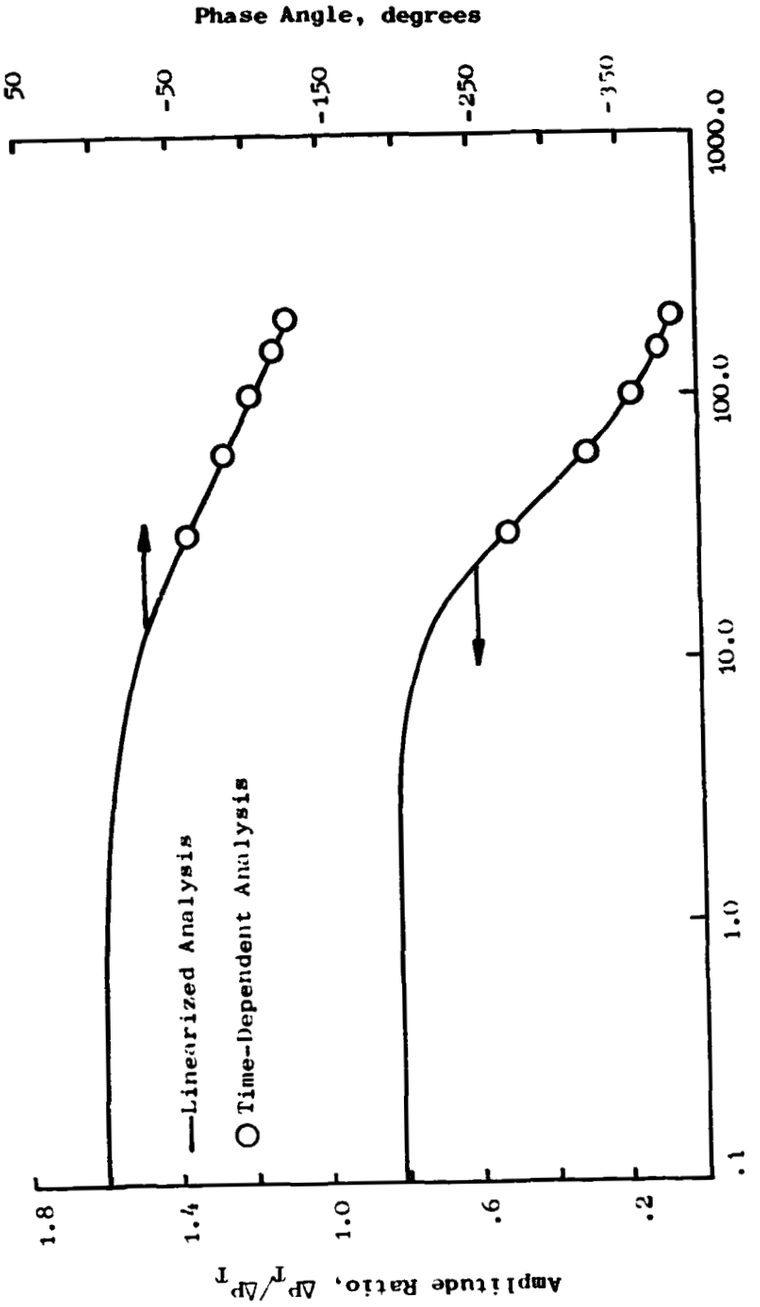

Figure 15. Compressor-Exit Total-Pressure Frequency Response To Inlet Total-Pressure Oscillation.

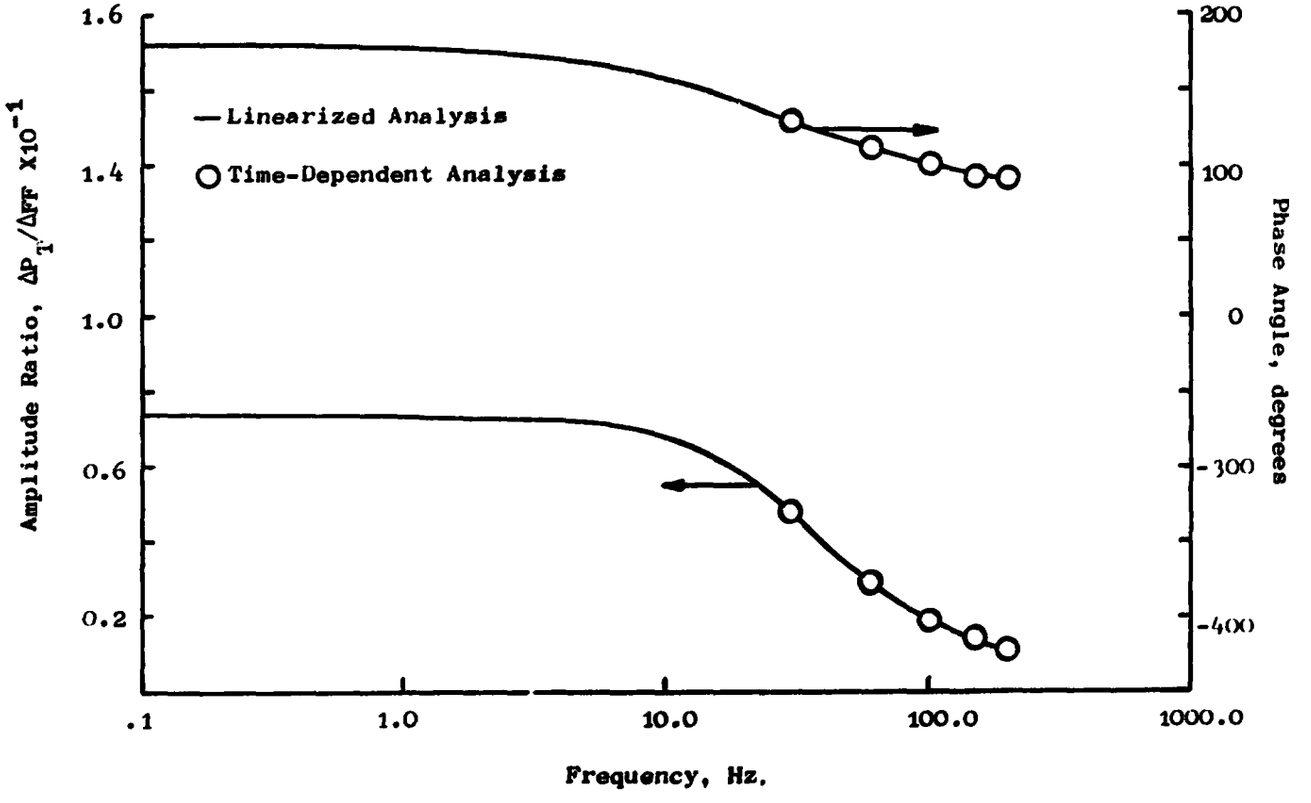

Figure 16. Compressor-Exit Total-Pressure Frequency Response To Combustor-Exit Flow-Function Oscillation.

loss in total pressure occurred as a result of the crossflow in the interstage axial gaps. The results of the distorted flow analysis with and without crossflow are discussed in the following paragraphs.

4.3.1 Parallel Compressor without Crossflow

During the NASA casing treatment program the J85-13 engine was tested with 1/rev circumferential total-pressure distortion generated by 42 percent (7-1/2 M) blockage screens with angular extents of 180°, 90°, 60°, and 30° and with 49 percent (9M) blockage screens with angular extents of 180°, 90°, and 60°. The results of this testing are reported in Reference 14.

These data were simulated using a two-sector parallel compressor model. The stability of the equations was determined using the A matrix formulation and actually calculating the roots of the characteristic equation. The roots were then examined to determine if a region of instability had been encountered as characterized by the presence of a positive real part of a root. The stability test was carried out for two levels of distortion (Table 2) at 80, 87, and 100 percent corrected speeds for the "Moss" engine. The stability tests were not carried out at 94% corrected speed since unexplainable results had been obtained at this speed line during clean-inlet-flow stability predictions.

The results of the moderate level of distortion (42 percent blockage) stability analyses are given in Figures 17 through 20 while the results for the high level (49 percent blockage) of distortion are given in Figures 21 through 23. The 180° 1/rev circumferential total-pressure distortion results of Figures 17 and 21 can be compared directly with the time-dependent model analysis of Reference 3. These comparisons show that the two methods give equivalent results. Examination of Figures 17 through 23 shows that the stability analyses of the two-sector parallel compressor model gave results which accurately reproduced the experimental speed lines at 80 and 87 percent corrected speeds, but at the higher level of distortion at 100 percent corrected speed, the flow shift to the low side was not being reproduced. All the results of Figures 17 through 23 show the typical classical parallel compressor results as far as predicting loss in surge pressure ratio, that is, it is predicted most accurately at high speeds where the speed lines are steep and it is overpredicted at the lower speeds and for low extent distortions.

The stability analysis method employed in this parallel compressor study offers economic advantages over the time-dependent model since its operating costs are approximately one-fifth of those incurred by the operation of the time-dependent model.

4.3.2 Parallel Compressor with Crossflow

In an effort to overcome the deficiencies of the parallel-compressor approach, that is, the overprediction of the loss in surge pressure ratio, it was hypothesized that inter-blade-row axial-gap crossflows might be the

Table 2. Measured Total-Pressure Distortion Levels.

		42% Blockage Screen (7-1/2 M)		49% Blockage Screen (9 M)	
% $N/\sqrt{\theta}$	Extent	$\Delta P_T/\bar{P}_T)_{Max}$*	$\Delta P_T/\bar{P}_T)_{Avg}$**	$\Delta P_T/\bar{P}_T)_{Max}$	$\Delta P_T/\bar{P}_T)_{Avg}$
100	180	0.1118	0.0559	0.1367	0.0683
	90	0.0918	0.0689	0.1114	0.0835
	60	0.0870	0.0725	0.1063	0.0885
	30	0.1009	0.0925	--	--
87	180	0.0594	0.0297	0.0677	0.0339
	90	0.0476	0.0357	0.0614	0.0461
	60	0.0446	0.0372	0.0558	0.0465
	30	0.0511	0.0468	--	--
80	180	0.0423	0.0212	0.0474	0.0237
	90	0.0351	0.0263	0.0428	0.0319
	60	0.0331	0.0276	0.0388	0.0323
	30	0.0373	0.0342	--	--

*$\Delta P_T/\bar{P}_T)_{Max} = (\overline{P_{T\ Max}} - \overline{P_{T\ Min}})/P_{T\ Avg}$

**$\Delta P_T/\bar{P}_T)_{Avg} = (P_{T\ Avg} - \overline{P_{T\ Min}})/P_{T\ Avg}$

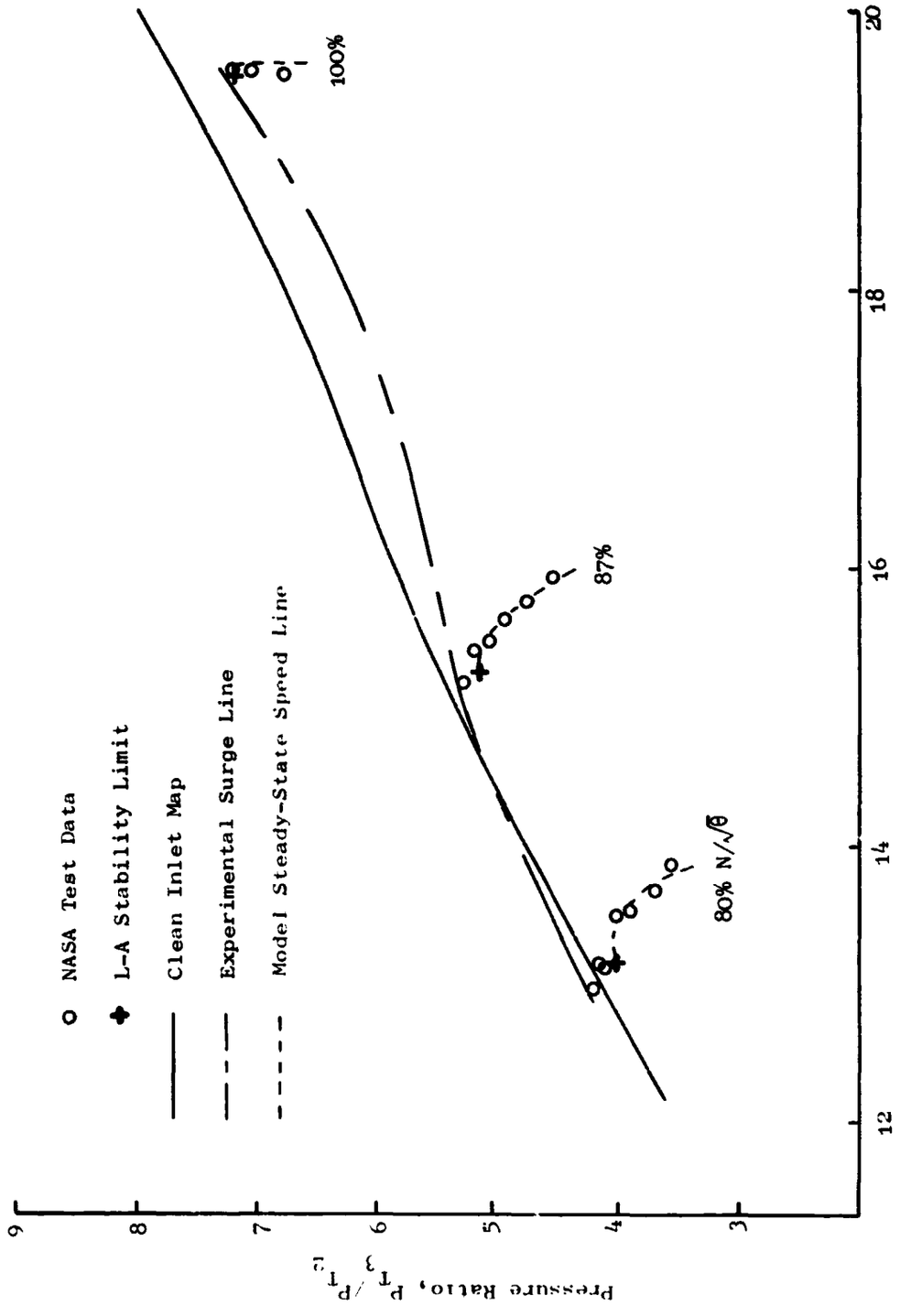

Figure 17. 180°, 1/Rev Total-Pressure Distortion (42% Blockage) Stability Analyses.

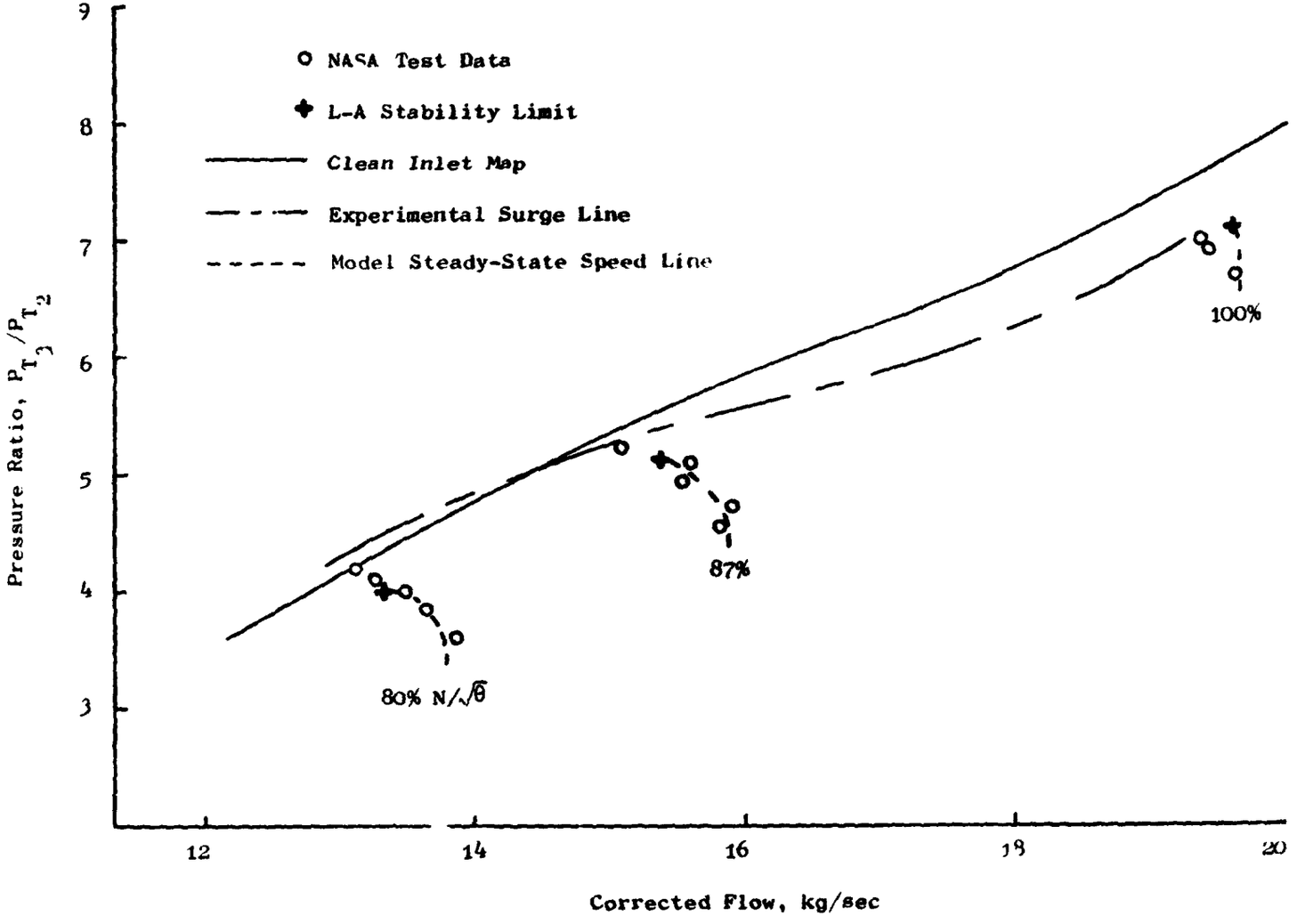

Figure 18. 90°, 1/Rev Total-Pressure Distortion (42% Blockage) Stability Analyses.

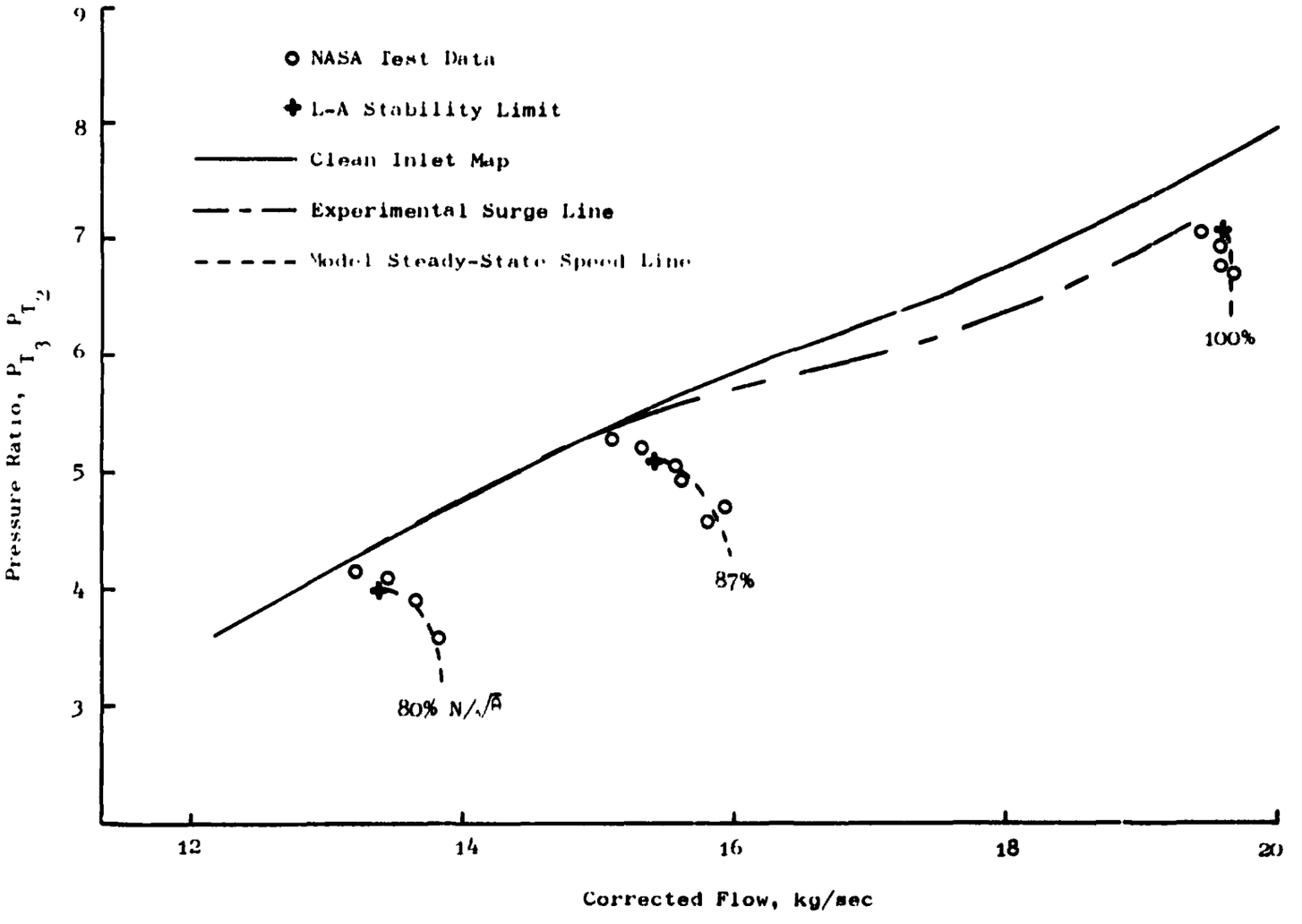

Figure 19. 60°, 1/Rev Total-Pressure Distortion (42% Blockage) Stability Analyses.

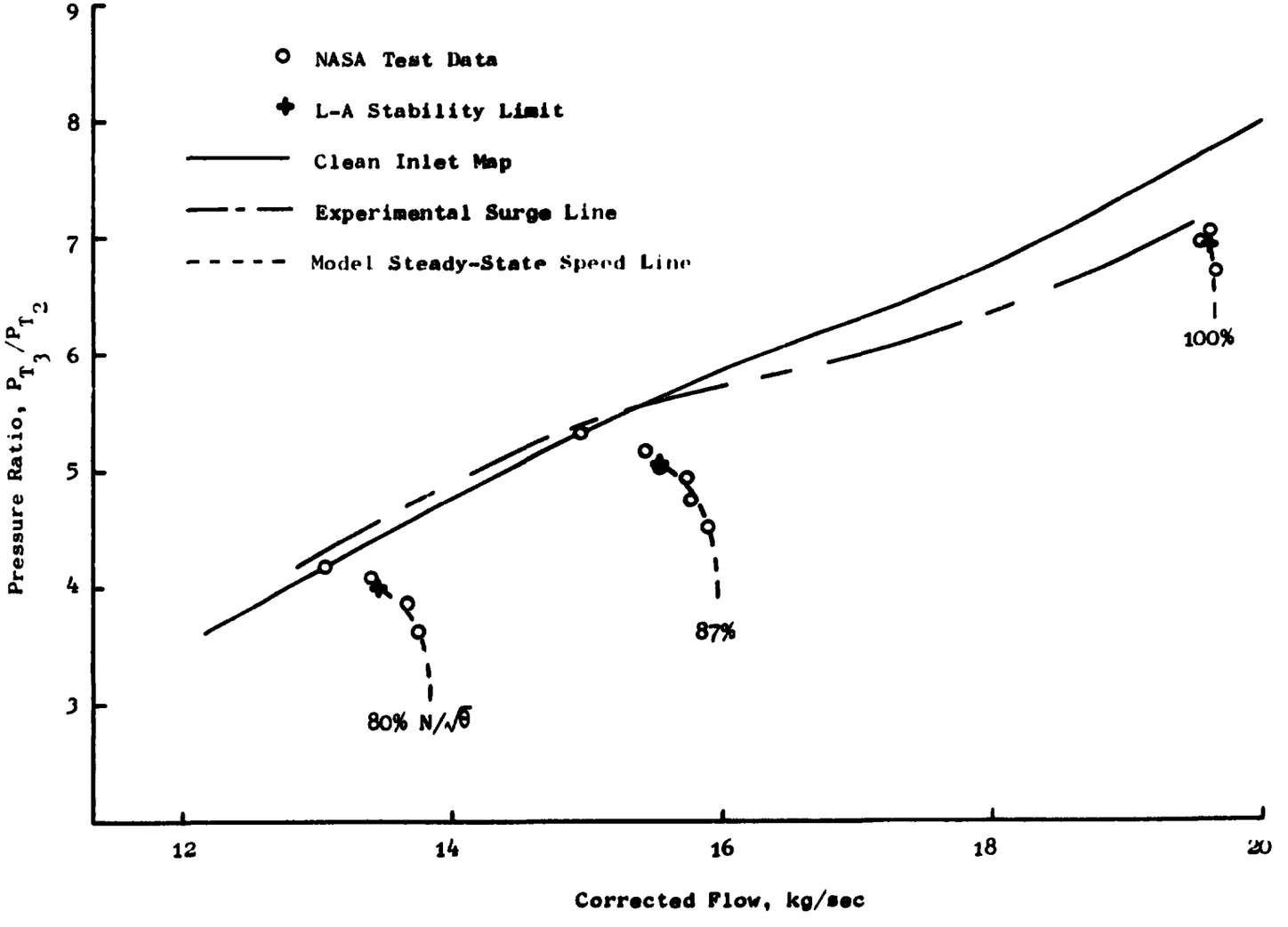

Figure 20. 30°, 1/Rev Total-Pressure Distortion (42% Blockage) Stability Analyses.

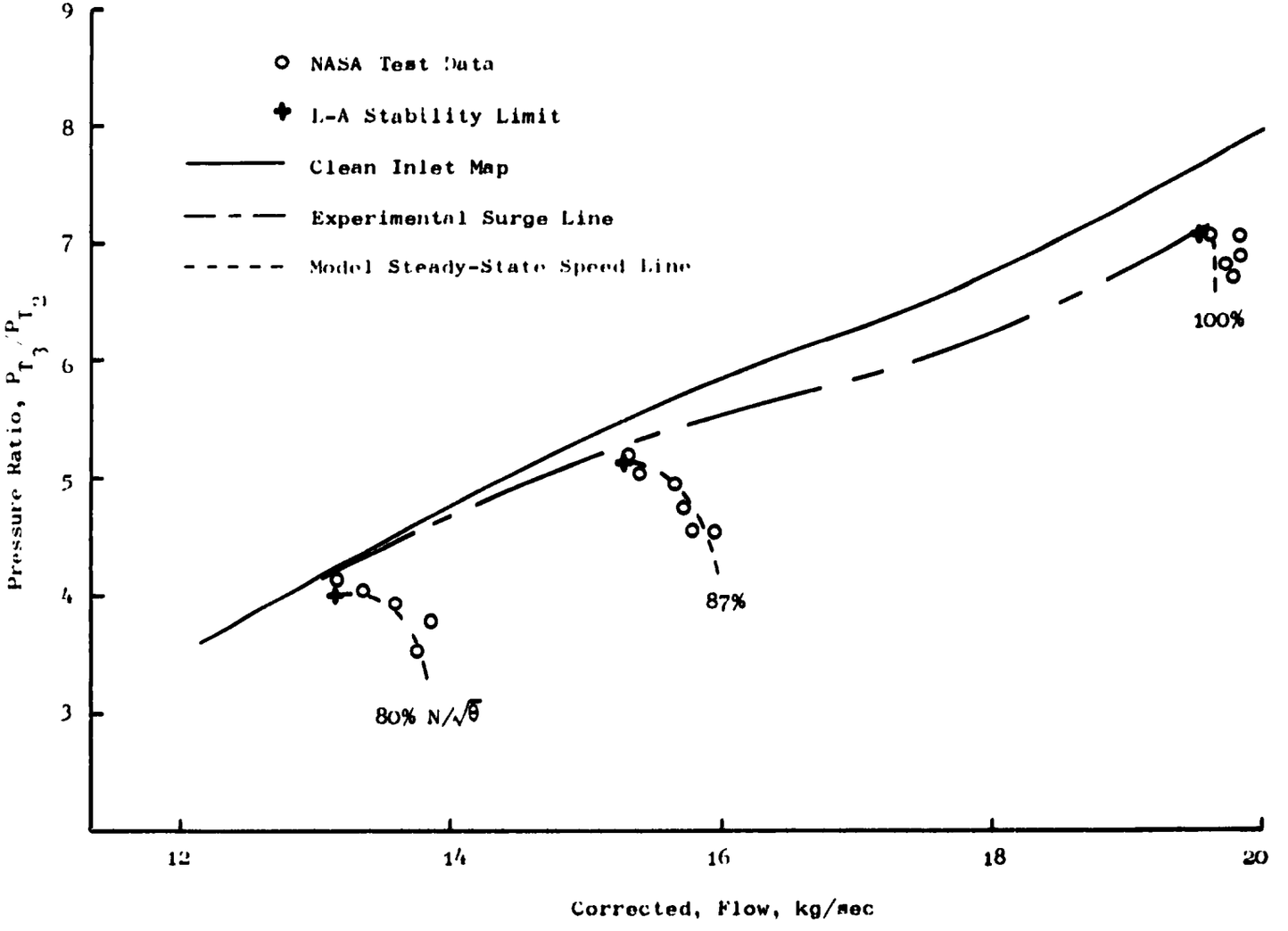

Figure 21. 180°, 1/Rev Total-Pressure Distortion (49% Blockage) Stability Analyses.

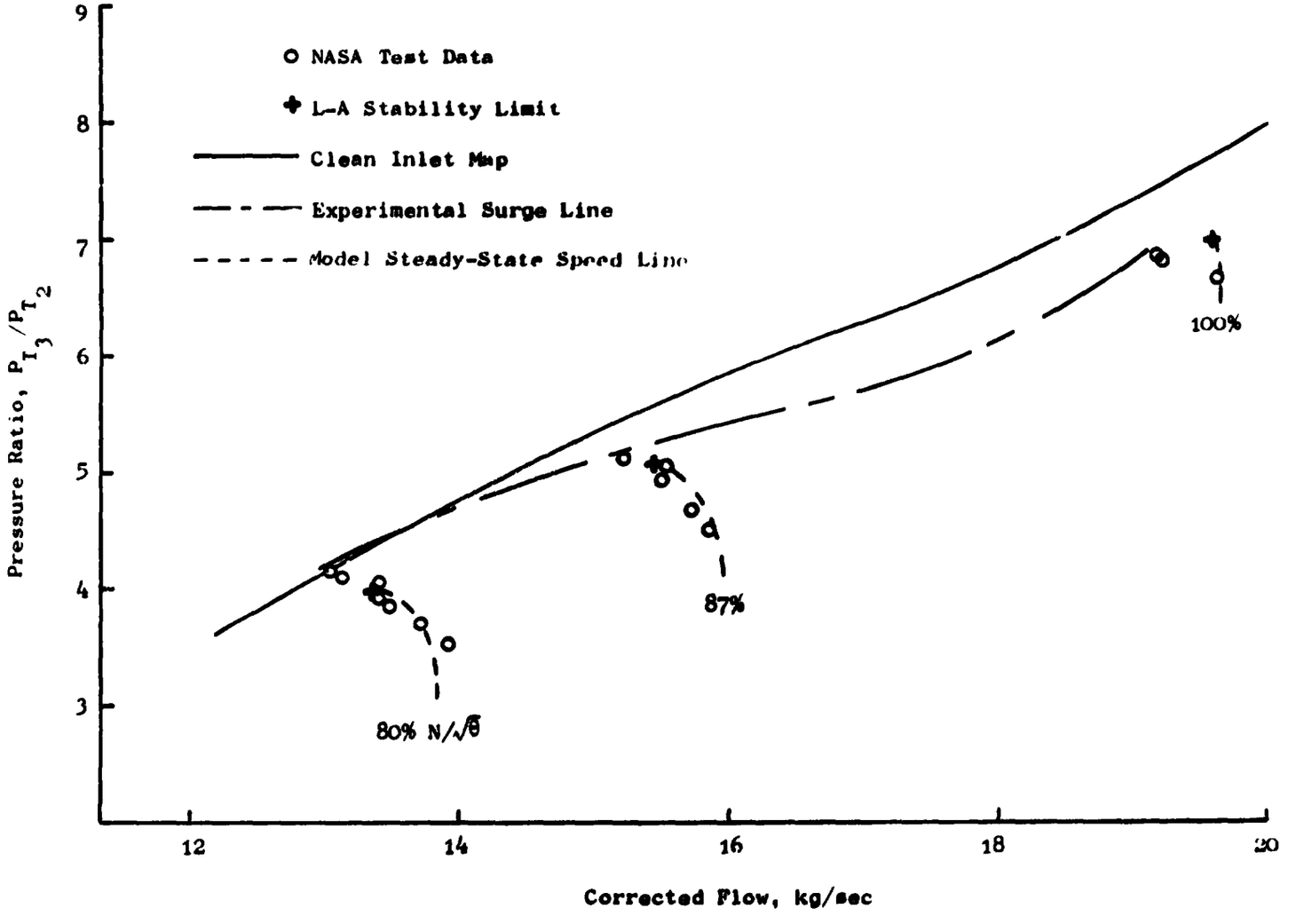

Figure 22. 90°, 1/Rev Total-Pressure Distortion (49% Blockage) Stability Analyses.

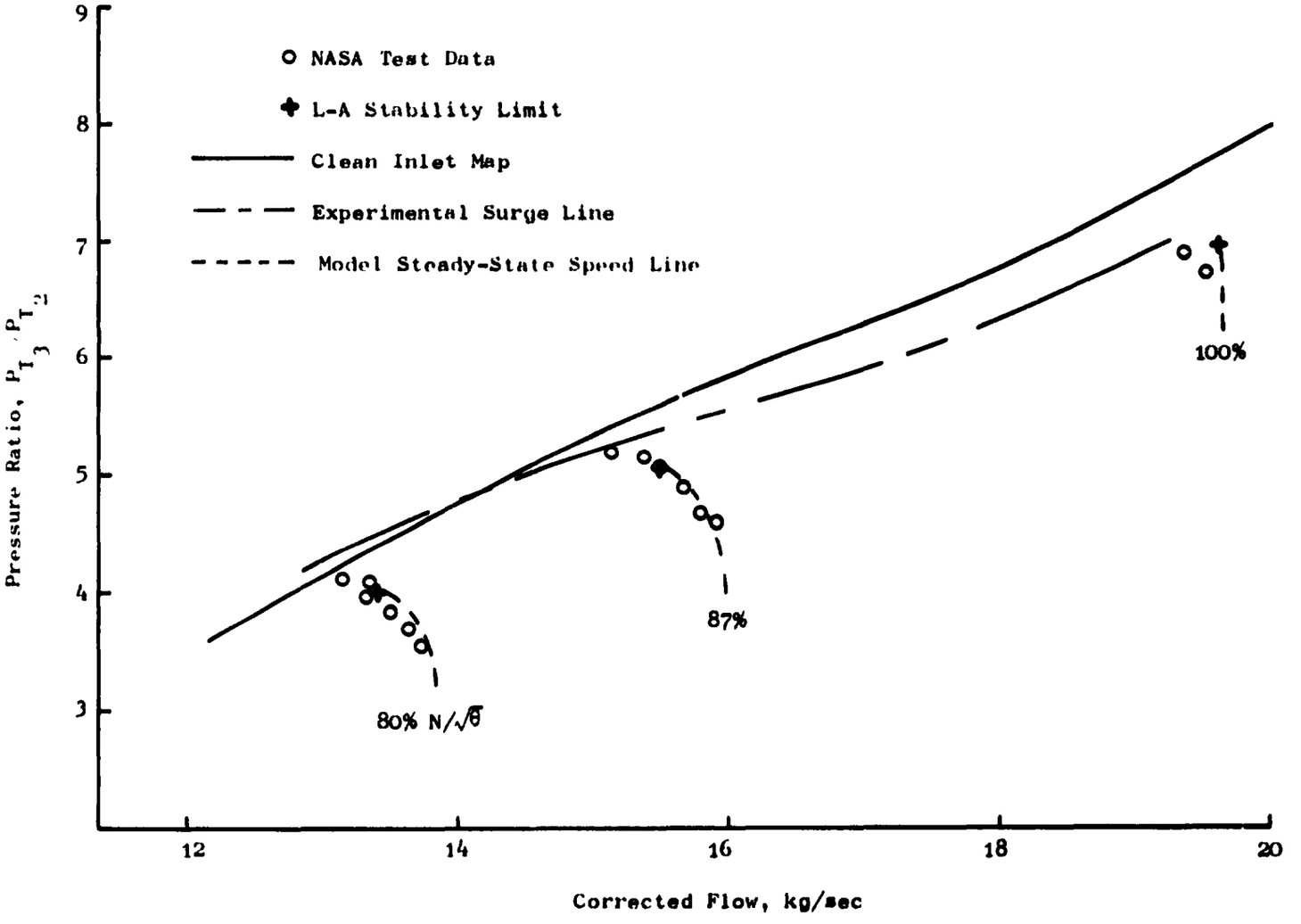

Figure 23. 60°, 1/Rev Total-Pressure Distortion (49% Blockage) Stability Analyses.

mechanism responsible for the loss in surge pressure ratio being less than predicted. The amount of crossflow was selected based upon matching measured internal-stage-distortion amplifications (Reference 15) at 80 and 100 percent corrected speeds for the 180° 1/rev high total-pressure distortion as shown in Figure 24. It was found that a crossflow of 1.2 and 1.0 percent of the undistorted sector inlet physical flow between stator 1 and rotor 2 at 80 and 100 percent corrected speeds, respectively, best matched the stage amplification data at the given operating point. The crossflow at 87 percent corrected speed was assumed to fall between the 80 and 100 percent values and was assumed to be 1.1 percent of sector inlet physical flow. Initially, the percentage crossflow for the other extents was established by multiplying the percentage crossflow at 180° by the ratio of the angular extent being simulated to 180° (ratio of the areas). However, this led to a speedline shape for the 30° extent distortion at 100 percent corrected speed which significantly departed from the experimentally determined speedline shape. The percentage crossflow was lowered for the 30° extent distortion until the speedline regained a proper shape. The percent crossflow at other speeds was lowered proportionately and the 180° and 30° points were connected by straight lines. This crossflow schedule as a percentage undistorted sector inlet physical flow is given in Figure 25.

The results of the crossflow studies are shown in Figures 26 through 29 for the 42 percent blockage screens and in Figures 30 through 32 for the 49 percent blockage screens. It is interesting to note that at 80 and 87 percent corrected speeds with the 42 percent blockage screens, only an insignificant increase in the predicted surge pressure ratio levels as compared to the levels without crossflow were noted. At 100 percent corrected speed, the introduction of crossflow worsens the data match and in fact causes an unrealistic hooking over of the mean speed line prior to indicating instability. This is due to the fact that stage one is forced to operate on the very low flow portion of its characteristics.

Essentially the same comments can be stated about the 49-percent-blockage-screen data except that at the low corrected speeds, the pressure ratio at instability is slightly lower.

In summary, it does not appear that the introduction of crossflow and its attendant mismatching of stages resulted in a better prediction of the loss of surge pressure ratio due to total-pressure distortion. It is possible that this result is biased by assuming a constant percentage of crossflow independent of operating line and/or by assuming that the shape of the attenuation characteristic (Figure 25) remains unchanged for extents of distortion less than 180 degrees.

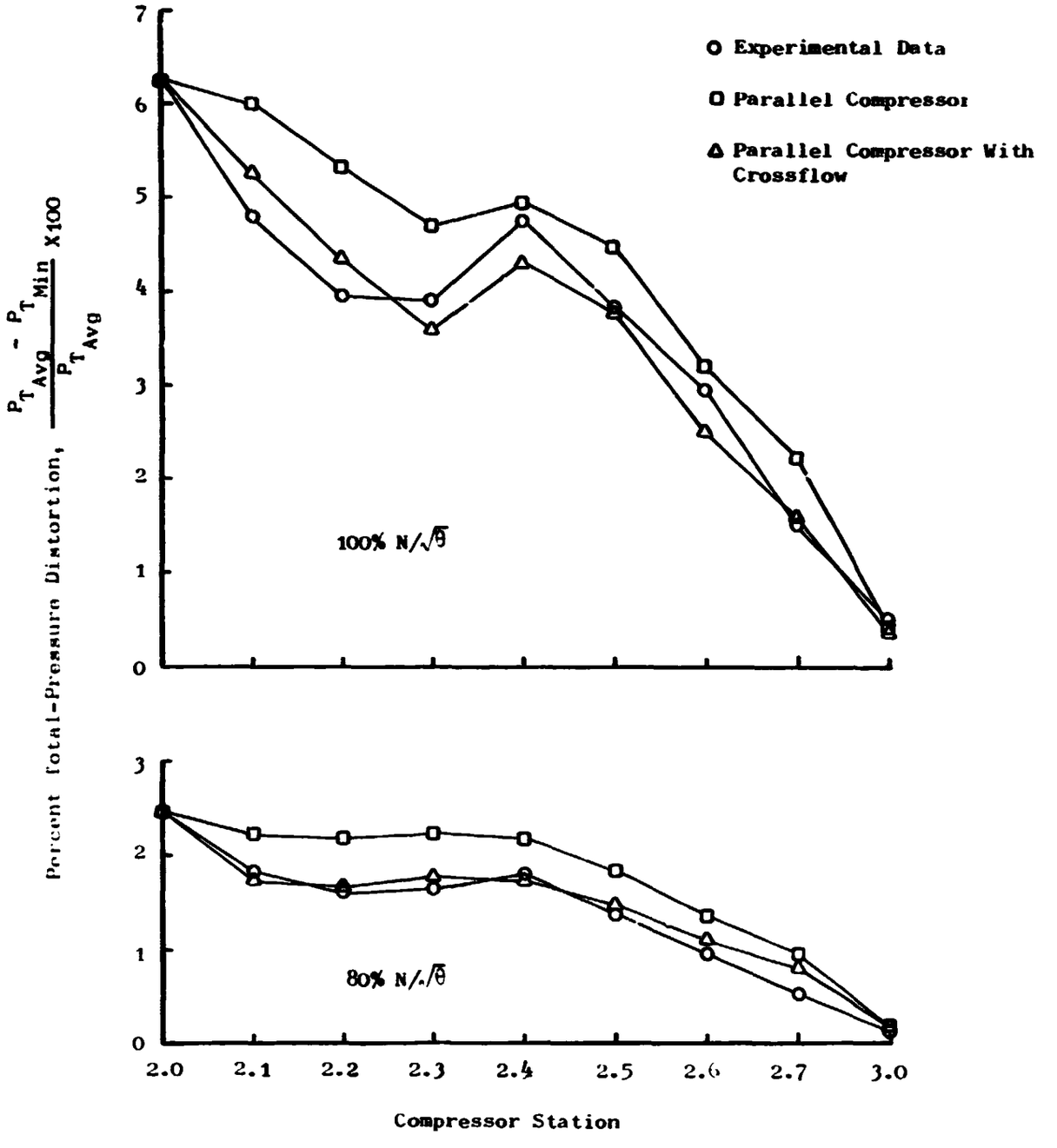

Figure 24. Effect of Interstage Crossflow on Distortion Attenuation Characteristics of 180° 1/Rev Total-Pressure Distortion.

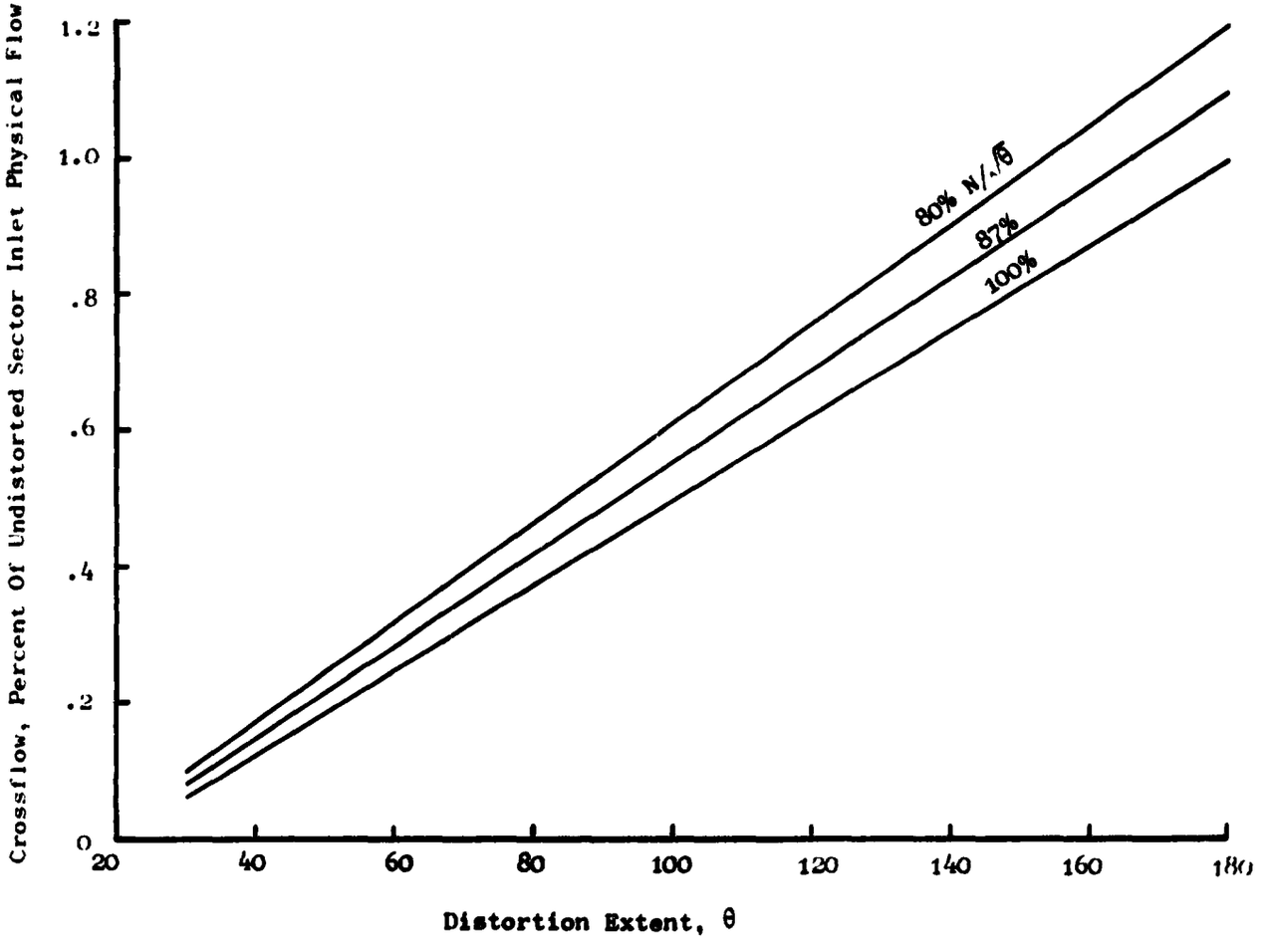

Figure 25. Crossflow Relationship to Distortion Extent and Corrected Speed.

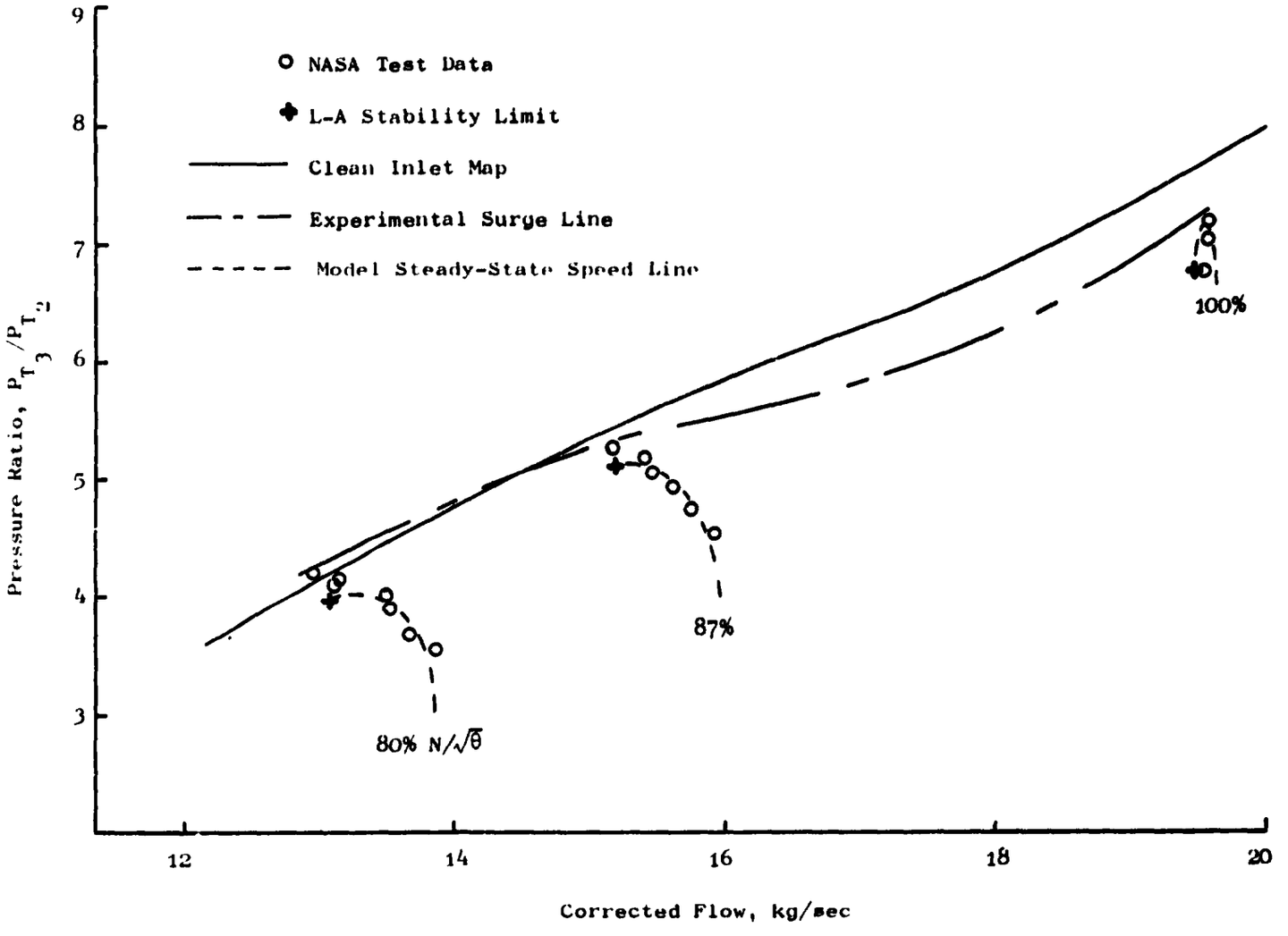

Figure 26. 180°, 1/Rev Total-Pressure Distortion (42% Blockage) With Interstage Crossflow Stability Analyses.

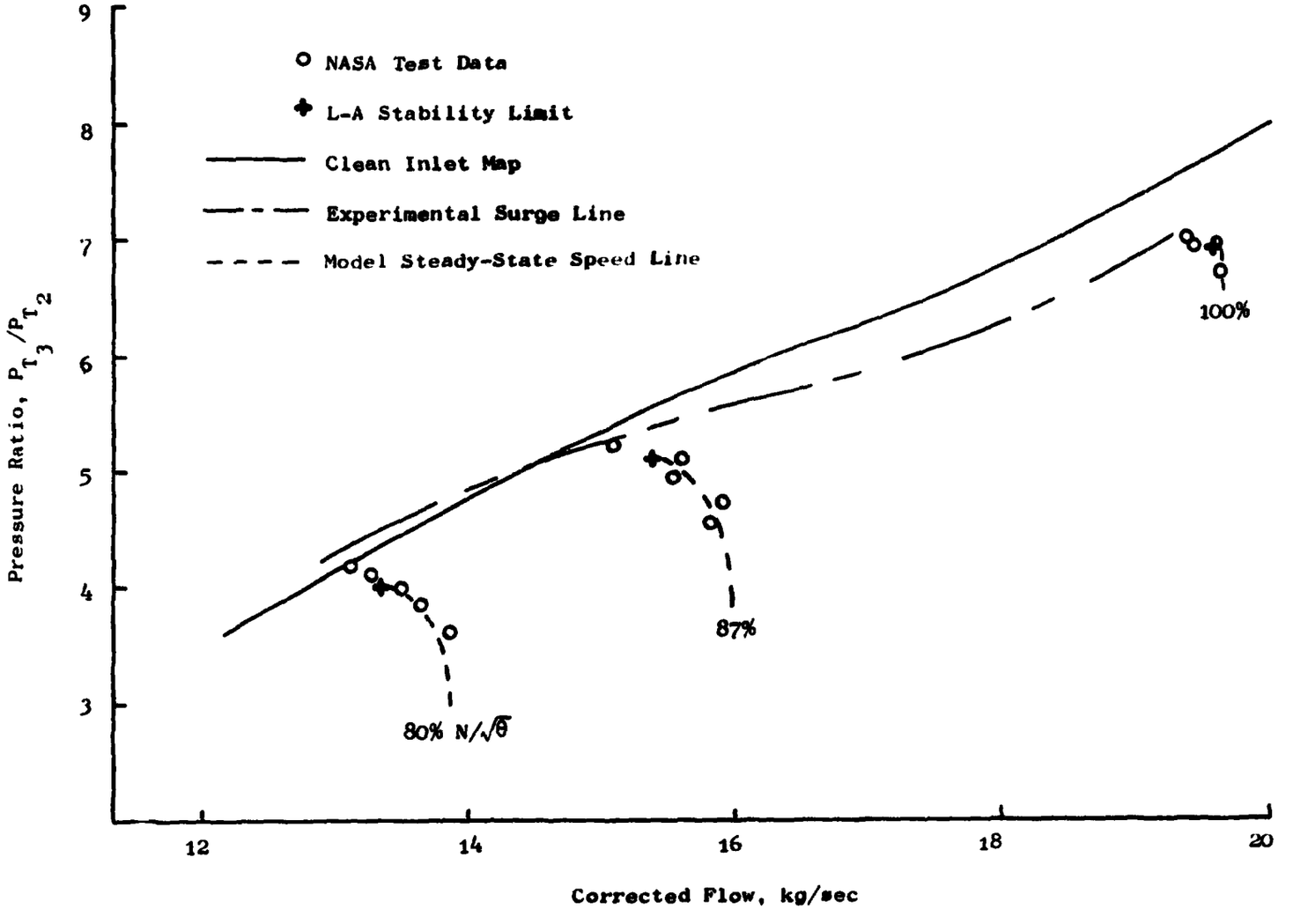

Figure 27. 90°, 1/Rev Total-Pressure Distortion (42% Blockage) With Interstage Crossflow Stability Analyses.

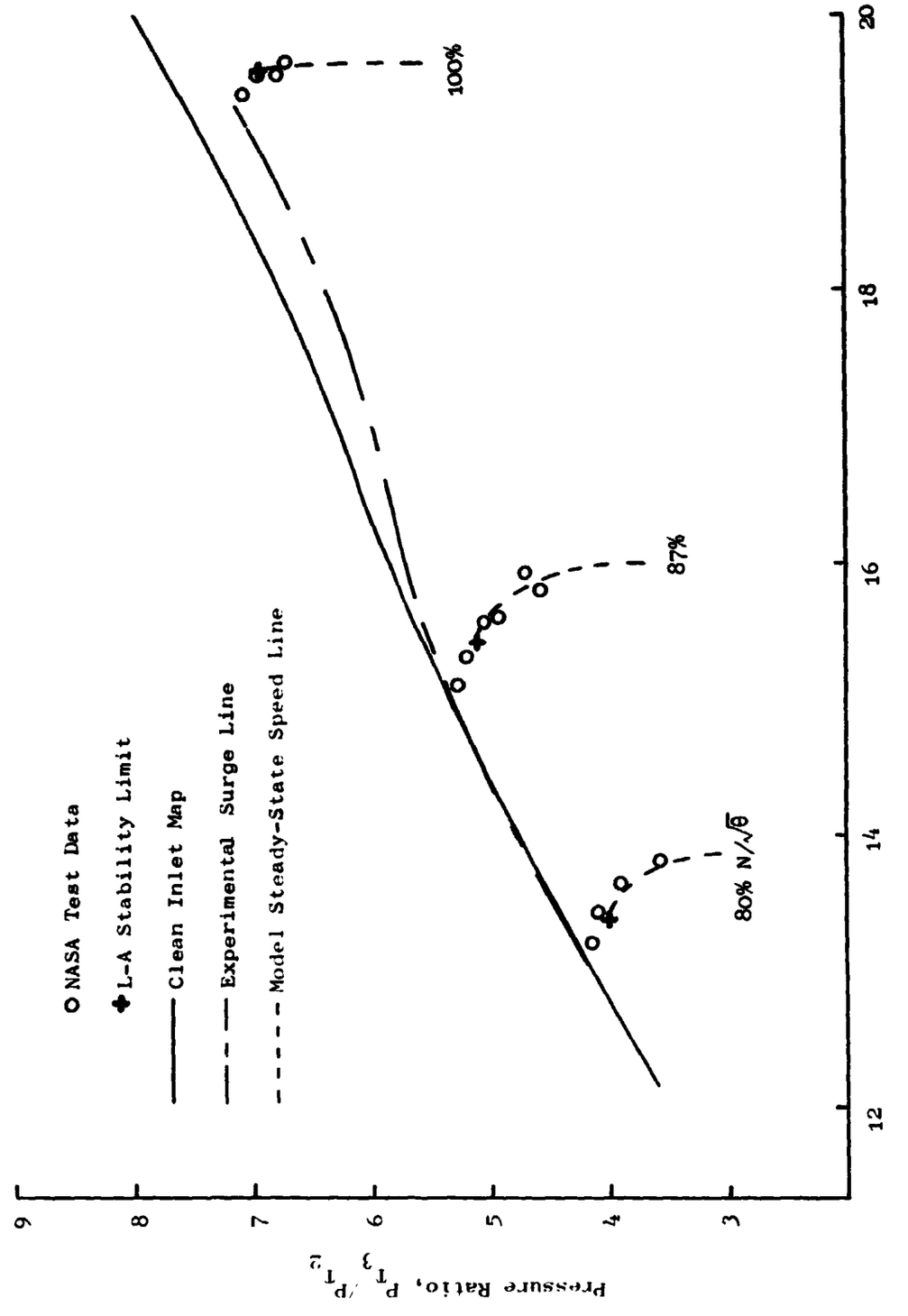

Figure 28. 60°, 1/Rev Total-Pressure Distortion (42% Blockage) With Interstage Crossflow Stability Analyses.

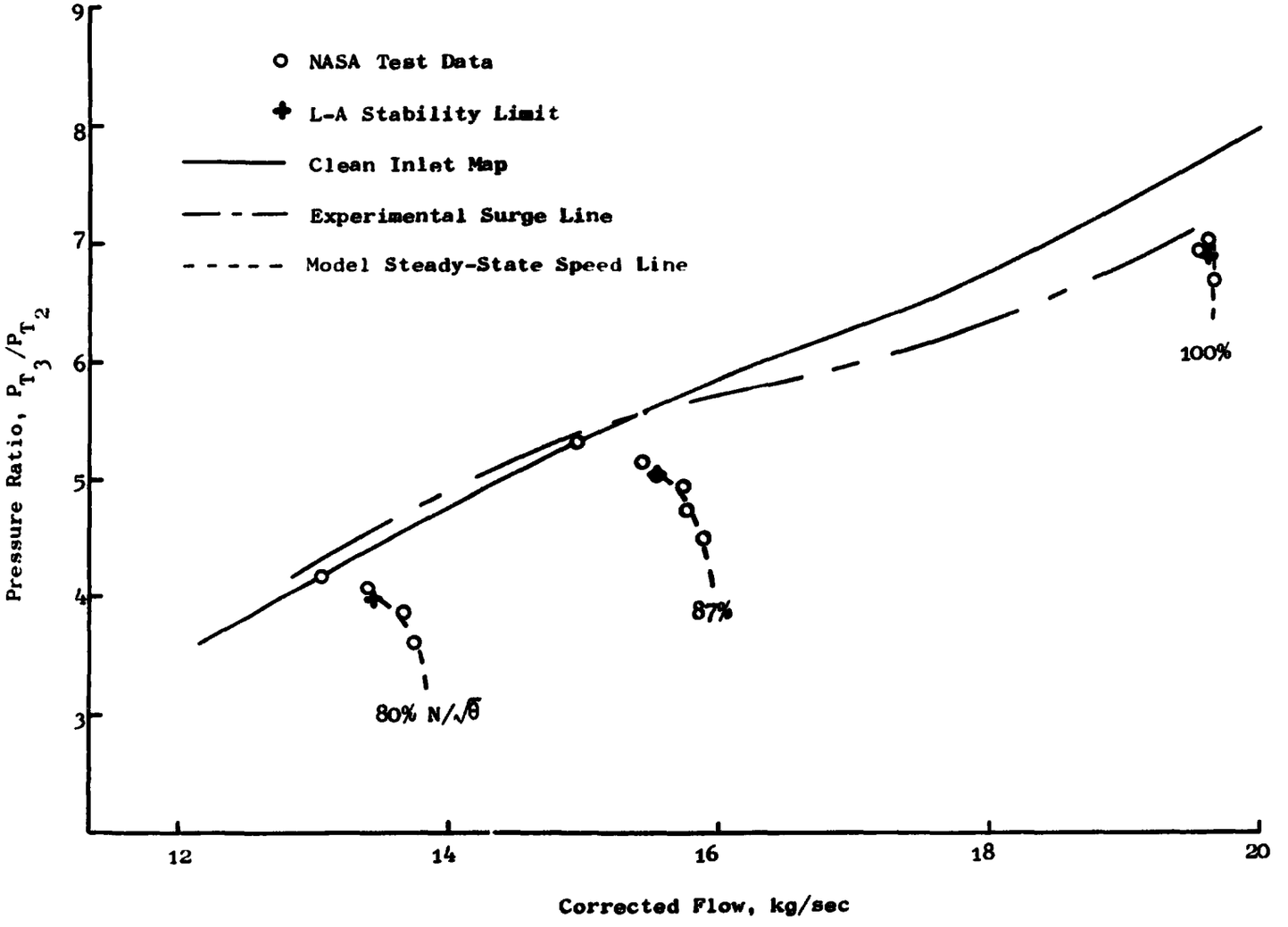

Figure 29. 30°, 1/Rev Total-Pressure Distortion (42% Blockage) With Interstage Crossflow Stability Analyses.

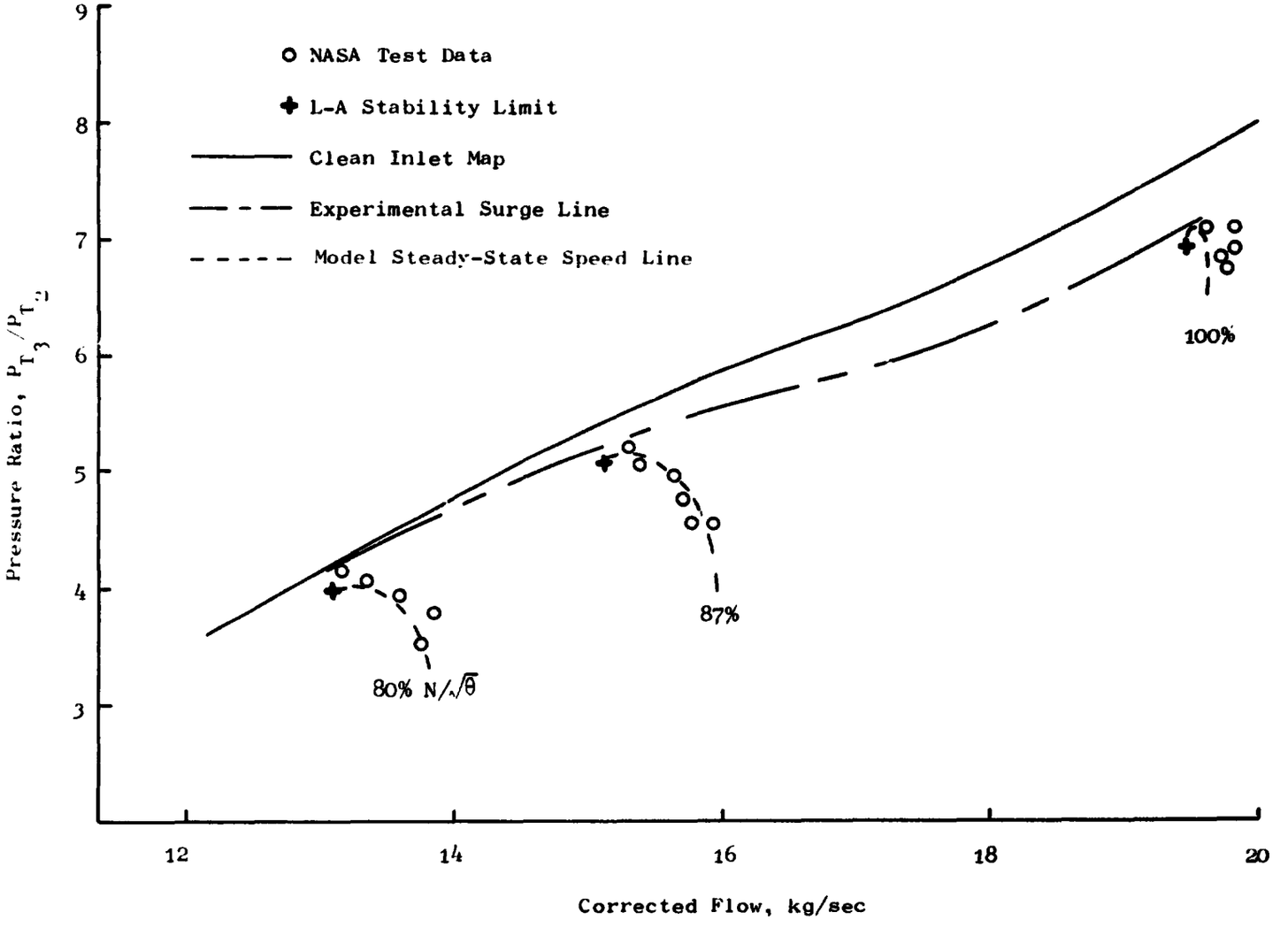

Figure 30. 180°, 1/Rev Total-Pressure Distortion (49% Blockage) With Interstage Crossflow Stability Analyses.

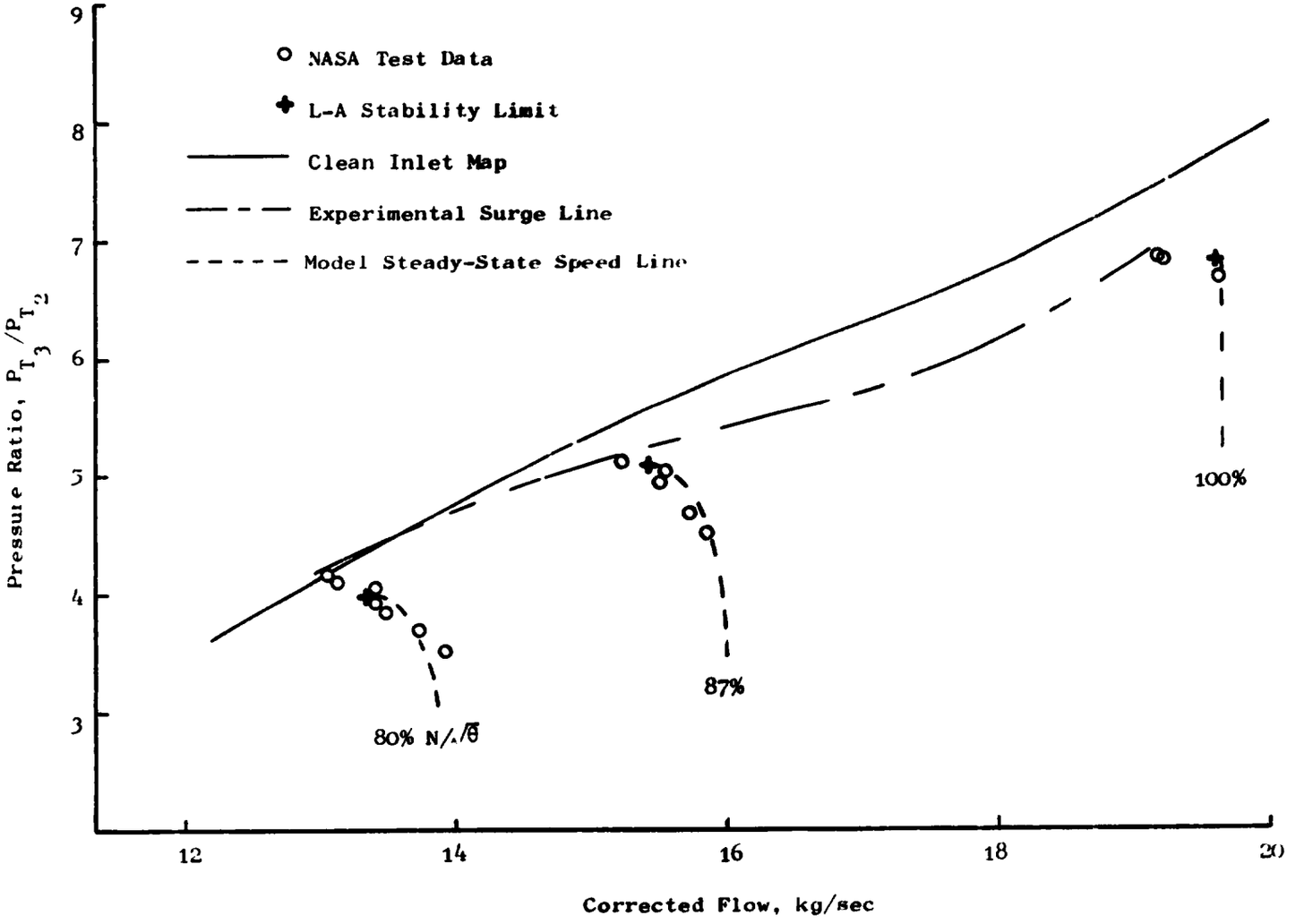

Figure 31. 90°, 1/Rev Total-Pressure Distortion (40% Blockage) With Interstage Crossflow Stability Analyses.

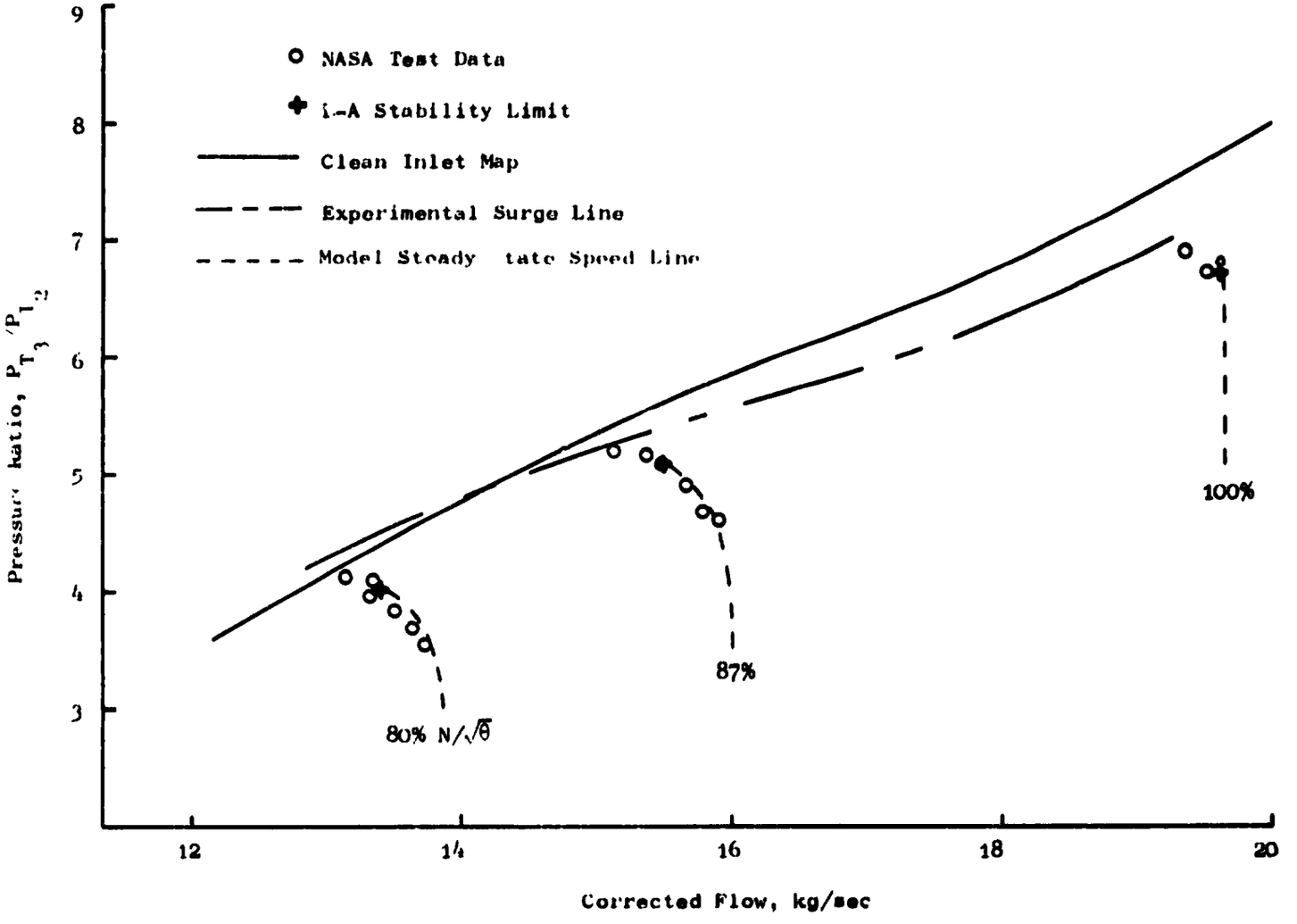

Figure 32. 60°, 1/Rev Total-Pressure Distortion (49% Blockage) With Interstage Crossflow Stability Analyses.

5.0 CONCLUSIONS AND RECOMMENDATIONS

This program is an example of the cross-fertilization of technology areas which must take place if progress is to continue and if a greater understanding of physical processes is to be obtained. In this case, linearized stability and frequency response analysis methods which are used primarily in control analyses are applied to the determination of gas-turbine-engine compressor-aerodynamic stability and frequency-response characteristics. The following conclusions can be drawn from the results of this study:

- The linearized stability analysis based upon the first method of Liapunov using the Jacobian $\underline{A}$ matrix and the alternate formulation of the Routh-Hurwitz stability criterion accurately reproduces the experimentally determined J85-13 clean-inlet-flow surge lines. These surge line results are also in close agreement (±0.05 kg/sec) with the results obtained from the time-dependent model of Reference 3.

- At 94% corrected speed for the "Moss" engine, surge is predicted at a pressure ratio lower than determined experimentally or predicted by the time-dependent model. Although great care was taken to insure accuracy, a small formulation error in the $\underline{A}$ matrix or a minor programming error cannot be ruled out at this time. Further, it is possible that assumptions introduced to permit linearizing the time-dependent model act to subtly decouple the stages and this decoupling is amplified by the character of the stage characteristics.

- The linearized-stability-analysis method offers clear economic advantages over the time-dependent model for clean-inlet-flow surge line determinations since its associated costs are one-fifteenth of those associated with the time-dependent model.

- The linearized-frequency-analysis technique produced results which accurately matched the time-dependent model up to nearly 200 Hz.

- Since it was determined that the linear analysis appeared to apply only for total-pressure oscillations on the order of ±0.5 percent of the mean inlet total pressure, great care must be exercised if the method is used to determine planar-wave dynamic distortion transfer coefficients since inlets of highly maneuverable aircraft may produce amplitudes on the order of ±10.0 percent of the mean inlet total pressure.

- Depending upon the frequency of interest and the number of stations where frequency responses are desired, there are economic tradeoffs which should be made before choosing either the linearized analysis

technique or the time-dependent method. In general if one or two discrete frequencies above 20 Hz are of interest, the time-dependent method is more economical. However, if a complete frequency response is of interest, then the linearized frequency response analysis is more economical.

- The linearized stability analysis of a two-sector blade row parallel compressor model gave results for 180° 1/rev inlet total-pressure distortions which reproduced the results obtained from the time-dependent model.

- The linearized stability analysis of the two-sector blade row parallel compressor model for the 180°, 90°, 60°, and 30° distortion extents give results which are typical of parallel compressors, that is, the loss in surge pressure ratio is overpredicted especially for the lower extents of distortion and for the lower speeds where the speed lines are of lower slope.

- Allowing for crossflow from the high total-pressure sector to the low-total pressure sector just downstream of stage 1 did not improve the accuracy of the loss in surge pressure ratio. In some cases the small amount of crossflow showed sufficient stage mismatch to force an unrealistic "hooking over" of the speed line prior to instability although stability predictions were made in this region.

- The costs of making a linearized stability analysis predictions of a two-sector parallel compressor are approximately one-fifth of those incurred by operating the time-dependent model. However, as the number of sectors increases, the $\underline{A}$ matrix used in making the linearized stability analysis becomes large very rapidly. Thus, when making a multisector parallel compressor analysis, it is necessary to evaluate whether the time-dependent approach may offer a more economical approach.

The linearized analysis stability prediction and frequency response techniques complement the time-dependent model technique and offer significant economic advantages when used in a judicious manner. It is envisioned that the two techniques would be used in the following manner. Clean surge line determinations would be accomplished using the linearized stability prediction technique. Frequencies at which amplifications occurred in a compressor component/ducting system would be determined by conducting linearized frequency response analyses over the frequency range of interest. At points where amplification is shown to occur, the time-dependent model would be employed with large amplitude boundary conditions to determine harmonic content, waveform shape, compression component planar-wave-transfer coefficients, etc. Where a two sector parallel compressor can provide an adequate estimate of loss in surge pressure ratio due to circumferential distortions, the linearized analysis stability prediction technique

would be employed. If it was deemed necessary to use a multi-sectored parallel compressor model, then it would be necessary to evaluate whether the linearized stability prediction technique or the time-dependent model offered economic advantages and to make the choice for usage accordingly.

The results of this study suggested areas that should receive further study. It is recommended that investigations be implemented to determine: 1) The validity of the linearized analysis stability model and/or its dependence on the number of stages operating on the positive portion of their characteristics, and 2) The potential existence of a physical interpretation of the eigenvalues that would be of benefit to the compressor designer.

APPENDIX A

JACOBIAN MATRIX FORMULATION

It was shown that the Jacobian (A) matrix (Equation 27) is a system of first partial derivatives of the mass, momentum and energy macrobalances with respect to the state variables $\bar{\rho}$, $\bar{W}$, and $\bar{s}$ at a steady-state operating point. Examination of the formulation of these partial derivatives revealed that they could be expressed explicity as a function of the state variables, thus, eliminating the need for finite difference approximations. This eliminates the dependence of the solution on perturbation size and thereby, eliminates a potential source of error.

Each station requires at least three known flow properties to define the state of the fluid. At an internal station, the station values are obtained by interpolating between adjacent volume averaged properties. The k-th volume fluid state is represented by the macrobalances of mass, momentum and energy (Equations 1, 2 and 3). A typical volume (k) with appropriate station notation (i) is shown in the following schematic:

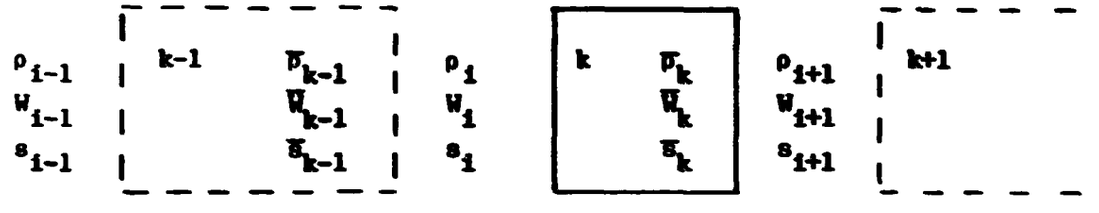

The set of three macrobalances for each volume is denoted by f_{3k-2}, f_{3k-1}, and f_{3k}, respectively, as shown by Equation 25. In these equations:

$$C_{z_i} = C_{z_i}(\rho_i, W_i) \tag{41}$$

$$P_i = P_i(\rho_i, s_i) \tag{42}$$

For stators,

$$F_{B_k} = F_{B_k}(\rho_{i-1}, W_{i-1}, \rho_i, W_i, \rho_{i+1}, W_{i+1}) \tag{43}$$

For rotors,

$$F_{B_k} = F_{B_k}(\rho_i, W_i, s_i, \rho_{i+1}, s_{i+1}) \tag{44}$$

For free volumes,

$$F_{B_k} = 0 \tag{45}$$

For rotors,

$$S_{F_k} = S_{F_k}(\rho_i, W_i, s_i, W_{i+1}) \tag{46}$$

For free volumes and stators,

$$S_{F_k} = 0 \tag{47}$$

The $\underline{A}$ matrix is of order 3k for a k volume compressor model. The partial derivatives of the functions f_{3k} are taken with respect to the volume-averaged state variables contained in its equation. Figure 33 shows a schematic representation of Volumes 4, 5 and 6 of the J85-13 compressor model. These volumes represent the IGV-trailing-edge free volume, stage 1 rotor and stage 1 stator, respectively. The continuity equation, in each case, has derivatives taken with respect to W_i and W_{i+1}.

$$\frac{\partial \dot{\rho}_k}{\partial W_i} = \frac{1}{V_k} \tag{48}$$

$$\frac{\partial \dot{\rho}_k}{\partial W_{i+1}} = \frac{1}{V_k} \tag{49}$$

The momentum equation provides derivatives of all surrounding state variables $(\rho_i, W_i, s_i, \rho_{i+1}, W_{i+1}, s_{i+1})$.

$$\frac{\partial \dot{W}_k}{\partial \rho_i} = -\frac{W_i^2}{\rho_i^2 A_i g_o} + \frac{\partial P_i}{\partial \rho_i} A_i - \frac{\partial P_M}{\partial \rho_i}(A_i - A_{i+1}) + \frac{\partial F_B}{\partial \rho_i} \tag{50}$$

$$\frac{\partial \dot{W}_k}{\partial W_i} = \frac{2W_i}{\rho_i A_i g_o} + \frac{\partial F_B}{\partial W_i} \tag{51}$$

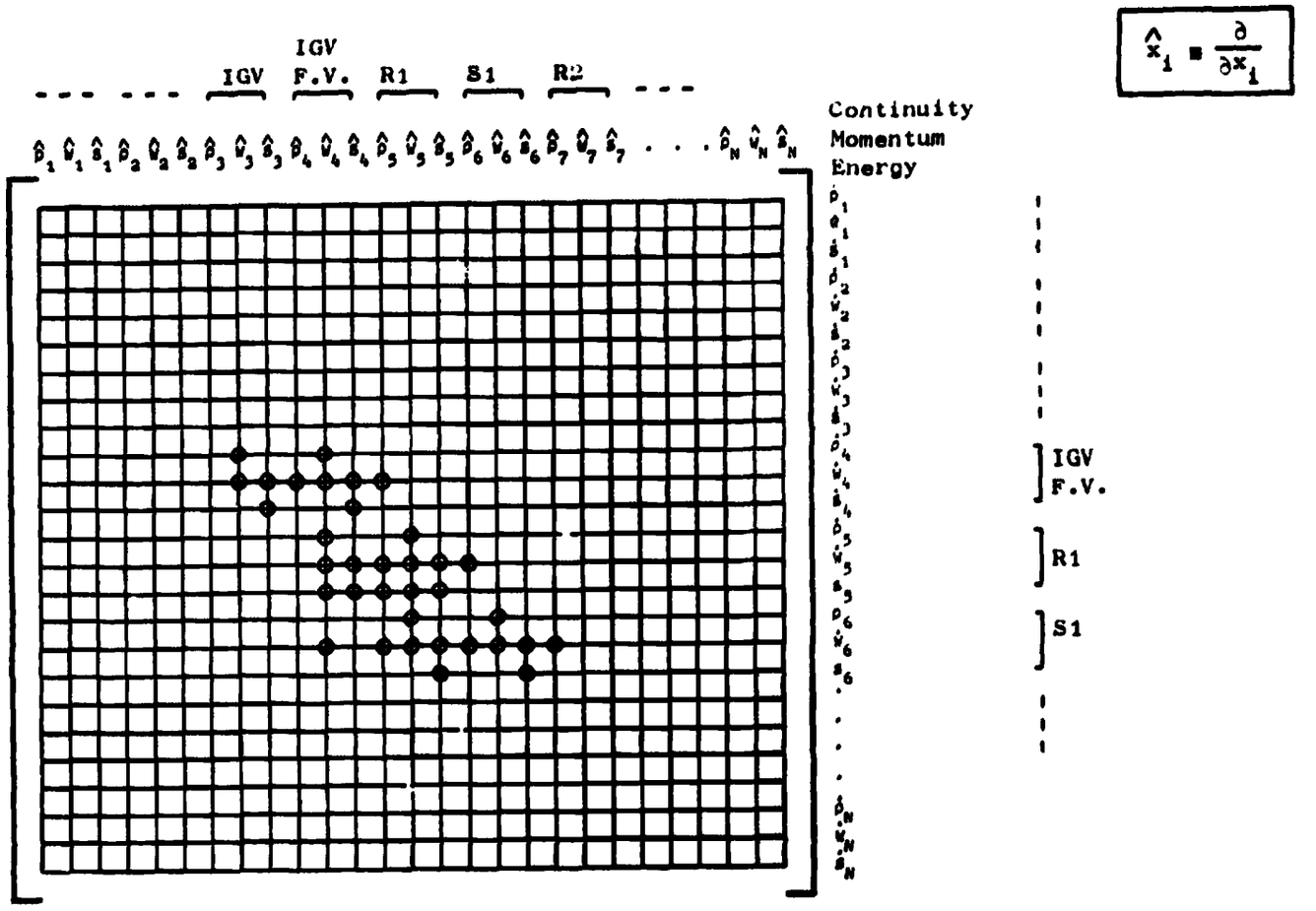

Figure 33. Jacobian Matrix Schematic.

$$\frac{\partial \dot{\bar{W}}_k}{\partial s_i} = \frac{\partial P_i}{\partial s_i} A_i - \frac{\partial P_M}{\partial s_i} (A_i - A_{i+1}) + \frac{\partial F_B}{\partial s_i} \tag{52}$$

$$\frac{\partial \dot{\bar{W}}_k}{\partial \rho_{i+1}} = \frac{W_{i+1}^2}{\rho_{i+1}^2 A_{i+1} g_o} - \frac{\partial P_{i+1}}{\partial \rho_{i+1}} A_{i+1} - \frac{\partial P_M}{\partial \rho_{i+1}} (A_i - A_{i+1}) + \frac{\partial F_B}{\partial \rho_{i+1}} \tag{53}$$

$$\frac{\partial \dot{\bar{W}}_k}{\partial W_{i+1}} = - \frac{2W_{i+1}}{\rho_{i+1} A_{i+1} g_o} + \frac{\partial F_B}{\partial W_{i+1}} \tag{54}$$

$$\frac{\partial \dot{\bar{W}}_k}{\partial s_{i+1}} = - \frac{\partial P_{i+1}}{\partial s_{i+1}} A_{i+1} - \frac{\partial P_M}{\partial s_{i+1}} (A_i - A_{i+1}) + \frac{\partial F_B}{\partial s_{i+1}} \tag{55}$$

Two additional derivatives are needed for stator volumes.

$$\frac{\partial \dot{\bar{W}}_k}{\partial \rho_{i-1}} = \frac{\partial F_B}{\partial \rho_{i-1}} \tag{56}$$

$$\frac{\partial \dot{\bar{W}}_k}{\partial W_{i-1}} = \frac{\partial F_B}{\partial W_{i-1}} \tag{57}$$

The energy equation provides derivatives taken with respect to s_i and s_{i+1}. However, for rotor volumes, the entropy production term (S_F) yields additional derivatives with respect to ρ_i, W_i, and W_{i+1}.

For free volumes and stators, $(s_{i+1} - s_i) = 0$

$$\frac{\partial \dot{\bar{s}}_k}{\partial s_i} = \frac{W_i}{\rho_i V_k} \tag{58}$$

$$\frac{\partial \dot{\bar{s}}_k}{\partial s_{i+1}} = - \frac{W_i}{\rho_i V_k} \tag{59}$$

For rotor volumes; $(s_{i+1} - s_i) \neq 0$

$$\frac{\partial \dot{s}_k}{\partial \rho_i} = \frac{1}{\rho_i^2 V_k} \left[- W_i (s_i - s_{i+1}) + \frac{\partial S_F}{\partial \rho_i} \right] \tag{60}$$

$$\frac{\partial \dot{s}_k}{\partial W_i} = \frac{1}{\rho_i V_k} \left[(s_i - s_{i+1}) + \frac{\partial S_F}{\partial W_i} \right] \tag{61}$$

$$\frac{\partial \dot{s}_k}{\partial s_i} = \frac{1}{\rho_i V_k} \left[W_i + \frac{\partial S_F}{\partial s_i} \right] \tag{62}$$

$$\frac{\partial \dot{s}_k}{\partial W_{i+1}} = \frac{1}{\rho_i V_k} \left[\frac{\partial S_F}{\partial W_{i+1}} \right] \tag{63}$$

$$\frac{\partial \dot{s}_k}{\partial s_{i+1}} = - \frac{W_i}{\rho_i V_k} \tag{64}$$

A general equation expressing static pressure in terms of static density and entropy can be easily derived.

$$P = P_{ref} \left(\frac{\rho}{\rho_{ref}} \right)^{\gamma} e^{(s - s_{ref})(\gamma-1)/R} \tag{65}$$

Derivatives of Equation 65 with respect to density and entropy are:

$$\frac{\partial P}{\partial \rho} = \frac{P\gamma}{\rho} \tag{66}$$

$$\frac{\partial P}{\partial s} = \frac{P(\gamma-1)}{R} \tag{67}$$

These equations lead directly to the formation of the derivatives of the P_M term.

For free volumes:

$$\frac{\partial P_M}{\partial \rho_i} = \frac{P_i \gamma}{\rho_i (1 + SF)} \tag{68}$$

$$\frac{\partial P_M}{\partial s_i} = \frac{P_i (\gamma-1)}{R (1 + SF)} \tag{69}$$

$$\frac{\partial P_M}{\partial \rho_{i+1}} = \frac{(SF) P_{i+1} \gamma}{\rho_{i+1} (1 + SF)} \tag{70}$$

$$\frac{\partial P_M}{\partial s_{i+1}} = \frac{(SF) P_{i+1} (\gamma-1)}{R (1 + SF)} \tag{71}$$

For rotors and stators:

$$\frac{\partial P_M}{\partial \rho_H} = \frac{2 P_H \gamma}{3 \rho_H} \tag{72}$$

$$\frac{\partial P_M}{\partial s_H} = \frac{2 P_H (\gamma-1)}{3 R} \tag{73}$$

$$\frac{\partial P_M}{\partial \rho_L} = \frac{P_L \gamma}{3 \rho_L} \tag{74}$$

$$\frac{\partial P_M}{\partial s_L} = \frac{P_L (\gamma-1)}{3 R} \tag{75}$$

where the subscripts H and L denote station parameters associated with the high and low pressures, respectively.

Equations 5 through 10 are expressions used for determining the blade force term (F_B). An expression relating absolute flow angle (α) to relative flow angle (β) in terms of local state variables can be derived.

$$\tan \beta = \frac{2\pi N r \rho A}{W} - \tan \alpha \tag{76}$$

Derivatives of the above equation and other fundamental relationships have been combined in the formulation of the blade force term derivatives and are shown in their final form below.

For stators:

$$\frac{\partial F_B}{\partial \rho_i} = F_T \frac{\partial (\tan \beta_\infty)}{\partial \rho_i} + \frac{\partial F_T}{\partial \rho_i} \tan \beta_\infty \tag{77}$$

$$\frac{\partial F_B}{\partial W_i} = F_T \frac{\partial (\tan \beta_\infty)}{\partial W_i} + \frac{\partial F_T}{\partial W_i} \tan \beta_\infty \tag{78}$$

$$\frac{\partial F_B}{\partial \rho_{i+1}} = \frac{\partial F_T}{\partial \rho_{i+1}} \tan \beta_\infty \tag{79}$$

$$\frac{\partial F_B}{\partial W_{i+1}} = \frac{\partial F_T}{\partial W_{i+1}} \tan \beta_\infty \tag{80}$$

$$\frac{\partial F_B}{\partial \rho_{i-1}} = F_T \frac{\partial (\tan \beta_\infty)}{\partial \rho_{i-1}} + \frac{\partial F_T}{\partial \rho_{i-1}} \tan \beta_\infty \tag{81}$$

$$\frac{\partial F_B}{\partial W_{i-1}} = F_T \frac{\partial (\tan \beta_\infty)}{\partial W_{i-1}} + \frac{\partial F_T}{\partial W_{i-1}} \tan \beta_\infty \tag{82}$$

For rotors:

$$\frac{\partial F_B}{\partial \rho_i} = F_T \frac{\partial (\tan \beta_\infty)}{\partial \rho_i} + \frac{\partial F_T}{\partial \rho_i} \tan \beta_\infty - \frac{\partial F_{DZ}}{\partial \rho_i} \tag{83}$$

$$\frac{\partial F_B}{\partial W_i} = F_T \frac{\partial(\tan \beta_\infty)}{\partial W_i} + \frac{\partial F_T}{\partial W_i} \tan \beta_\infty - \frac{\partial F_{DZ}}{\partial W_i} \tag{84}$$

$$\frac{\partial F_B}{\partial s_i} = - \frac{\partial F_{DZ}}{\partial s_i} \tag{85}$$

$$\frac{\partial F_B}{\partial \rho_{i+1}} = \frac{\partial F_T}{\partial \rho_{i+1}} \tan \beta_\infty \tag{86}$$

$$\frac{\partial F_B}{\partial W_{i+1}} = \frac{\partial F_T}{\partial W_{i+1}} \tan \beta_\infty \tag{87}$$

Equation 12 is an expression for the entropy production term (S_F) in the energy equation and represents the blade row losses in rotor volumes.

$$\frac{\partial S_F}{\partial \rho_i} = \frac{W_{i+1}{}^R}{P_{r_I} P_{r_A}} \left(P_{r_A} \frac{\partial P_{r_I}}{\partial \rho_i} - P_{r_I} \frac{\partial P_{r_A}}{\partial \rho_i} \right) \tag{88}$$

$$\frac{\partial S_F}{\partial W_i} = \frac{W_{i+1}{}^R}{P_{r_I} P_{r_A}} \left(P_{r_A} \frac{\partial P_{r_I}}{\partial W_i} - P_{r_I} \frac{\partial P_{r_A}}{\partial W_i} \right) \tag{89}$$

$$\frac{\partial S_F}{\partial s_i} = \frac{W_{i+1}{}^R}{P_{r_I} P_{r_A}} \left(P_{r_A} \frac{\partial P_{r_I}}{\partial s_i} - P_{r_i} \frac{\partial P_{r_A}}{\partial s_i} \right) \tag{90}$$

$$\frac{\partial S_F}{\partial W_{i+1}} = R \ln \left(\frac{P_{r_I}}{P_{r_A}} \right) \tag{91}$$

where:

$$P_{r_I} = \left(\frac{P'_{T_2}}{P'_{T_1}} \right)_{ideal} \tag{92}$$

$$P_{r_A} = \left(\frac{P'_{T_2}}{P'_{T_1}} \right)_{actual} \quad (93)$$

Hence, Equations 48 through 93 completely define the elements of the Jacobian matrix.

Boundary conditions were imposed at the compressor-model inlet and exit volumes. It was previously mentioned that each station requires at least three known flow properties to define the state of the fluid. Model-inlet total pressure and total temperature are imposed explicitly as boundary conditions, while the density is implied. At the model exit flow function was specified in a manner analogous to specifying a choked exit boundary condition, while the flow and entropy were implied.

A parallel compressor model based upon an extension of the Dynamic Blade Row Compression Component Stability Model was used for the distorted-inlet-flow studies. Parallel compressor theory is based on the assumption that each sector operates on its clean inlet characteristics and exits to a uniform static-pressure interface downstream of the compressor exit guide vanes. Flow from each sector is summed prior to entering the downstream volume and the entropy is implied. Inlet and exit boundary conditions are identical to those used in the clean-inlet-flow model.

APPENDIX B

FREQUENCY RESPONSE INPUT MATRIX FORMULATION

The analytical formulation of the partial derivatives of the input response (B) matrix is analogous to the methods, previously described in Appendix A. For a k - volume system, partial derivatives of the macrobalances of mass, momentum and energy are taken with respect to each input (u_n) while holding all state variables constant. The resulting matrix is of the form

$$\underline{B} = \begin{bmatrix} \frac{\partial f_1}{\partial u_1} & \cdots & \frac{\partial f_1}{\partial u_n} \\ \vdots & & \vdots \\ \frac{\partial f_{3k}}{\partial u_1} & \cdots & \frac{\partial f_{3k}}{\partial u_n} \end{bmatrix} \tag{94}$$

The two inputs used in this study are the compressor inlet total pressure and the compressor exit flow function. Consequently, the inlet and exit free volumes, respectively, are the only volumes containing these input parameters. All $\underline{B}$ matrix elements associated with the remaining volumes are zero.

The first column of the $\underline{B}$ matrix contains the partial derivatives of the state equations with respect to inlet total pressure. The continuity and momentum equations (Equations 1 and 2), of the first volume, provide the only non-zero elements for the input total-pressure oscillation. In these equations for this particular volume, station subscript "i" corresponds to the compressor inlet station, where

$$W_i = W_{inlet}\ (P_{t_{inlet}}) \tag{95}$$

$$P_i = P_{inlet}\ (P_{t_{inlet}}) \tag{96}$$

Expressions for the above equations can be easily derived. The resulting partial derivatives of the static equations are

$$\frac{\partial \dot{\rho}_1}{\partial P_{t_i}} = \frac{1}{V_K} \frac{\partial W_i}{\partial P_{t_i}} \tag{97}$$

$$\frac{\partial \dot{W}_1}{\partial P_{t_i}} = \frac{g_o}{L_K}\left[\frac{2\, W_i \dfrac{\partial W_i}{\partial P_{t_i}}}{g_c \rho_i A_i} + \frac{\partial P_i}{\partial P_{t_i}} A_i - \frac{\partial P_M}{\partial P_{t_i}} (A_i - A_{i+1})\right] \tag{98}$$

$$\frac{\partial \dot{s}_i}{\partial P_{t_i}} = 0 \tag{99}$$

The second column of the $\underline{B}$ matrix contains derivatives with respect to exit flow function. The momentum equation associated with the last free volume provides the only non-zero elements. At the terminating station, static density and pressure are expressed in terms of the local flow function.

$$\rho_{i+1} = \rho_{exit}\,(FF) \tag{100}$$

$$P_{i+1} = P_{exit}\,(FF) \tag{101}$$

All matrix elements associated with the continuity and energy equations are zero. The resulting partial derivatives are of the form

$$\frac{\partial \dot{\rho}_k}{\partial FF} = 0 \tag{102}$$

$$\frac{\partial \dot{W}_k}{\partial FF} = \frac{g_o}{L_k}\left[\frac{W_{i+1}^2}{g_o \rho_{i+1}^2 A_{i+1}} \frac{\partial o_{i+1}}{\partial FF} - \frac{\partial P_{i+1}}{\partial FF} A_{i+1} + \frac{\partial P_M}{\partial FF} (A_i - A_{i+1})\right] \tag{103}$$

$$\frac{\partial \dot{s}_k}{\partial FF} = 0 \tag{104}$$

Once the input response matrix is generated, all scale factors applied to the $\underline{A}$ matrix must be applied to the $\underline{B}$ matrix and the frequencies used to evaluate the frequency response characteristics.

APPENDIX C

DESCRIPTION OF MATRIX TRANSFER FUNCTION SOLUTION TECHNIQUE

Given the $\underline{A}$, $\underline{B}$, and $\underline{C}$ matrices (Equations 28 and 29) of appropriate dimension, the problem is to obtain the matrix transfer function given by Equation 33

$$\frac{\underline{R}(s)}{\underline{U}(s)} = \underline{C}(s\underline{I} - \underline{A})^{-1}\,\underline{B}$$

The technique that has been programmed in Reference 8 considers only one element of the matrix at a time. For example, consider the scalar transfer function between the i-th element of $\underline{R}$ (r) and the j-th element of $\underline{U}$ (u).

$$\frac{r}{u} = \underline{C}_i\,(s\underline{I} - \underline{A})^{-1}\,\underline{B}_j \tag{105}$$

where $\underline{C}_i$ is the i-th row of $\underline{C}$ and $\underline{B}_j$ is the j-th column of $\underline{B}$.

The problem is simplified by using the transform given in Reference 16 since it will eliminate the need for a $\underline{C}_i$ vector by making the output r a state variable in the transformed system.

$$\underline{F} = \underline{T}\,\underline{B}_j \tag{106}$$

$$\underline{G} = \underline{T}\,\underline{Y} \tag{107}$$

$$\underline{E} = \underline{T}\,\underline{A}\,\underline{T}^{-1} \tag{108}$$

such that

$$\dot{\underline{G}} = \underline{E}\,\underline{G} + \underline{F}\,u \tag{109}$$

where $\underline{T}$ is the identify matrix except that the MC-th row is overwritten by the $\underline{C}_i^T$ vector. The integer MC is the position of the element of $\underline{C}_i$ with the maximum absolute value. The $\underline{T}^{-1}$ matrix is similar to inverses encountered in the proof of the Danilevsky method (see Reference 9) and can be written down explicitly. The output r of the unmodified system is the MC-th modified state variable G_{MC}. Thus Equation 105 b comes:

$$\frac{\underline{r}}{u} = (s\,\underline{I} - \underline{E})^{-1}\,\underline{F} \tag{110}$$

or

$$(s\,\underline{I} - \underline{E})\underline{r} = \underline{F}\,u \tag{111}$$

This is a matrix of linear equations and in theory can be solved by Cramer's rule. The solution is

$$\frac{\underline{r}}{u} = \frac{\det\,(\underline{W})}{\det\,(s\,\underline{I} - \underline{E})} \tag{112}$$

where $\underline{W}$ is the system Wronskian obtained by replacing the MC-th column of $(s\,\underline{I}-\underline{E})$ with the $\underline{F}$ vector. The determinant of $(s\,\underline{I}-\underline{E})$ equals the determinant of $(s\,\underline{I}-\underline{A})$ and is the characteristic polynomial of the system $\underline{A}$ matrix. The Danilevsky method provides an efficient algorithm for obtaining the characteristic polynomial (see Reference 9). It uses similarity transformations to put the matrix in a phase variable form where a row of the transformed $\underline{A}$ matrix becomes the characteristic polynominal. The determinant of $\underline{W}$ is found using a clever algorithm developed by Bollinger (Reference 17). Using a few properties of determinants, he derived a method for evaluating the determinant of $\underline{W}$ using two evaluations of the Danilevsky type expressions: (1) The denominator polynomial is the characteristic equation of the system transfer function and is obtained by the Danilevsky method using the $\underline{A}$ or $\underline{E}$ matrix and (2) The numerator polynomial is obtained in two more characteristic polynomial calculations using Bollinger's method. The first characteristic polynomial is obtained by replacing the MC-th column of $\underline{E}$ by $-\underline{F}$ to obtain Z2; the second characteristic polynomial is obtained through use of a matrix of order (n-1) and is obtained by deleting the MC-th row and column from $\underline{E}$ to obtain Z3. The numerator polynomial is computed as

$$\det\,(\underline{W}) = Z2 - Z3 \tag{113}$$

Thus, system transfer function is written as

$$\frac{\underline{r}(s)}{u(s)} = \frac{\det\,(\underline{W})}{\det\,(s\,\underline{I} - \underline{A})} \tag{114}$$

REFERENCES

1. Willoh, R.G., and Seldner, K., "Multistage Compressor Simulation Applied to the Prediction of Axial Flow Instability," National Aeronautics and Space Administration Technical Memorandum NASA TM X-1880, 1969.

2. Gray, W.G., "Propulsion System Flow Stability Program (Dynamic), Phase I Final Technical Report, Part V. Models for Predicting Compressor Response to Spatial and Time-Variant Distortion - Basic Theory and Comparisons of Model and Test Data," Air Force Aero Propulsion Laboratory Technical Report AFAPL TR-68-142, Part V, December 1968.

3. Tesch, W.A., and Steenken, W.G., "Blade Row Dynamic Digital Compressor Program, Volume I, J85 Clean Inlet Flow and Parallel Compressor Models," National Aeronautics and Space Administration Contractor Report NASA CR-134978, 197t.

4. Daniele, C.J., Blaha, R.J., and Seldner, K., "Prediction of Axial-Flow Instabilities in a Turbojet Engine by Use of a Multistage Compressor Simulation on The Digital Computer," National Aeronautics and Space Administration Technical Memorandum NASA TM X-3144, 1975.

5. Daniele, C.J., And Teren, F., "Prediction of Compressor Stall for Distorted and Undistorted Flow by Use of a Multistage Compressor Simulation on the Digital Computer," National Aeronautics and Space Administration Technical Memorandum TM X-71633, 1975.

6. Reynolds, G.G., and Steenken, W.G., "Dynamic Digital Blade Row Compression Component Stability Model - Model Validation and Analysis of Planar Pressure Pulse Generator and Two-Stage Fan Test Data," Air Force Aero-Propulsion Laboratory Report AFAPL-TR-76-76, August 1976.

7. Ogata, K., State Space Analysis of Control Systems, Prentice-Hall, 1967.

8. Seidel, R.C., "Computer Programs for Calculation of Matrix Stability and Frequency Response From a State - System Description," National Aeronautics and Space Administration Technical Memorandum NASA TM X-71581, 1974.

9. Faddeeva, V.N., Computational Methods of Linear Algebra, Dover, 1959.

10. Korn, G.A., and Korn, T.M., Mathematical Handbook For Scientists and Engineers, Second Edition, McGraw-Hill, 1961.

11. Wilkinson, J.H., The Algebraic Eigenvalue Problem, Oxford, 1965.

12. Wenzel, L.M., Moss, J.E. Jr., and Mehalic, C.M , "Effect of Casing Treatment on Performance of a Multistage Compressor," National Aeronautics and Space Administration Technical Memorandum NASA TM X-3175, 1975.

13. Mehalic, C.M., and Lottig, R.A., "Steady-State Inlet Temperature Distortion Effects on the Stall Limits of a J85-GE-13 Turbojet Engine," National Aeronautics and Space Administration Technical Memorandum TM X-2990, 1974.

14. Milner, E.J., and Wenzel, L.M., "Performance of a J85-13 Compressor with Clean and Distorted Inlet Flow," National Aeronautics and Space Administration Technical Memorandum NASA TM X-3304, 1975.

15. de Bogdan, C.E., Moss, J.E. Jr., and Braithwaite, W.M., "Internal Flow Characteristics of a Multistage Compressor With Inlet Pressure Distortion," National Aeronautics and Space Administration Technical Memorandum NASA TM X-3446, 1977.

16. Davison, E.J., "A Computational Method for Finding the Zeros of a Multivariable Linear Time Ivariant System," Automatica, v6,n3, May 1970. pp. 481-484.

17. Bollinger, K.E., and Mathur, J.C., "To Compute the Zeros of Large Systems," IEEE Trans, vAC-16, n1, February 1971, pp. 95-96.